

~~Stream discharge depends more on the~~**Effects of spatial and** ~~temporal distribution of variability in surface water inputs~~⁴
~~than on yearly snowfall fractions for a headwater catchment at~~**on streamflow generation and cessation in** ~~the rain-snow~~
~~transition zone.~~

~~Leonie Kiewiet~~^{1,2}, ~~Ernesto Trujillo~~^{3,4}, ~~Andrew Hedrick~~⁴, ~~Scott Havens~~⁴, ~~Katherine Hale~~^{5,6}, ~~Mark Seyfried~~⁴, ~~Stephanie~~
~~Kampf~~^l, ~~Sarah E. Godsey~~²

¹ Department of Ecosystem Science and Sustainability, Colorado State University, Fort Collins, CO, USA

² Department of Geosciences, Idaho State University, Pocatello, ID, USA

³ Department of Geosciences, Boise State University, Boise, ID, USA

⁴ USDA Agricultural Research Service, Boise, ID, USA

⁵ Department of Geography, University of Colorado, Boulder, CO, USA

⁶ Institute of Arctic and Alpine Research, University of Colorado, Boulder, CO, USA

Abstract

~~Climate warming~~**change** ~~affects snowfall fractions and snowpack storage, displaces the rain-snow transition zone towards~~
~~higher elevations, and impacts discharge~~**precipitation phase, which can propagate into changes in streamflow** ~~timing and~~
~~magnitude as well as low-flow patterns. However, it remains unknown. This study examines~~ how variations in the spatial and
~~temporal distribution of precipitation at the rain-snow transition zone~~**rainfall and snowmelt** ~~affect discharge. To investigate~~
~~this, we in rain-snow transition zones. These zones experience large year-to-year variations in precipitation phase, cover a~~
~~significant area of mountain catchments globally, and might extend to higher elevations under future climate change. We used~~
~~observations from eleven weather stations and snow depths measured in~~**from** ~~one aerial lidar survey to force a spatially~~
~~distributed snowpack model (iSnohal/Automated Water Supply Model) in a semi-arid, 1.8 km² headwater catchment at the~~
~~rain-snow transition zone.~~ We focused on surface water inputs (SWI; the summation of rainfall and snowmelt **on the soil**) for
four years with contrasting climatological conditions (wet, dry, rainy and snowy) and compared simulated SWI to measured
discharge. ~~We obtained a~~**A** ~~strong spatial agreement between snow depth from the lidar survey and model (r²: -0.88), and was~~
~~observed, with~~ a median Nash-Sutcliffe Efficiency (NSE) of 0.65 for simulated and measured snow depths for all modelled
years (0.75 for normalized snow depths). The spatial pattern of SWI was consistent between the four years, with north-facing
slopes producing 1.09 to 1.25 times more SWI than south-facing slopes, and snow drifts producing up to six times more SWI
than the catchment average. ~~We found that~~**Annual** ~~discharge in a snowy year the catchment was almost twice as high as in a~~
~~rainy year, despite similar SWI. However, years not significantly correlated~~ ~~with a lower snowfall the~~ ~~fraction did not always~~
~~have lower annual discharge nor earlier stream drying. Instead, we found that~~**of precipitation falling as snow, but instead with**
~~the magnitude of precipitation and spring snow and rain. Stream cessation depended total and spring precipitation, but also on~~
~~snowpack characteristics:~~ the dry-out date ~~at the catchment outlet~~ was positively correlated to the snowpack melt-out date.
These results highlight the **importance of the** heterogeneity of SWI at the rain-snow transition zone **for streamflow generation**
and cessation, and emphasize the need for spatially distributed modelling or monitoring of both ~~the~~ snowpack and rainfall
dynamics.

Keywords: snowfall fraction, SWI, SWE, **recharge**, streamflow, dry-out date, non-perennial, satellite, iSnohal

Style Definition: Normal (Web)

Formatted: Font: Bold

Formatted: Normal, Line spacing: single

Formatted: Font: Bold

Formatted: Font: Bold

Formatted: English (United States)

Formatted: Font color: Auto

Formatted: Font color: Auto, Superscript

Formatted: Font color: Auto

Formatted: Font: 8 pt

1. Introduction

Due to increases in temperature, mountainous regions will receive less snowfall and more rainfall (Barnett et al., 2005; Stewart, 2009). This will alter the timing and amount of snowmelt, a significant source for water resources across the globe (Barnett et al., 2005; Marks et al., 1999; Somers and McKenzie, 2020; Viviroli et al., 2007). On the scale of the continental United States (US), a decrease in the fraction of precipitation falling as snow (snowfall fraction hereinafter) is expected to decrease stream discharge (Berghuijs et al., 2014). Earlier stream discharge peaks in response to earlier snowmelt and a decline in summer low flows across the semi-arid mountainous US have been reported in both observational data records (McCabe et al., 2017; Luce and Holden, 2009; Regonda et al., 2005) and future climate projections (Naz et al., 2016; Leung et al., 2004; Milly and Dunne, 2020; Christensen et al., 2004). However, lower snowfall fractions in much of the western United States have not yet led to a significant decrease in annual discharge (McCabe et al., 2017). Given that future climate predictions suggest further low-flow declines are likely, understanding year-round discharge responses, and in particular the sensitivity of stream discharge to changes in yearly snowfall fractions, is therefore warranted, and will help us to anticipate how stream discharge might be affected by climate change.

Variations in snowfall fractions can affect the temporal distribution of surface water inputs (SWI = rainfall + snowmelt onto the soil). Snowpacks store water and release snowmelt later, whereas rain on snow-free ground immediately enters the hydrologic system. After rainfall or snowmelt reaches the ground surface, it might become stream discharge, remain stored on the land surface or in the soil, recharge deeper groundwater, or become evaporated or transpired. Generally, water inputs from rain or snowmelt during periods with high antecedent wetness and low evapotranspiration rates are more likely to recharge groundwater and generate discharge (Jasechko et al., 2014; Molotch et al., 2009; Hammond et al., 2019). Rainfall and snowmelt inputs might result in similar runoff ratios (discharge/SWI) as long as the overall catchment wetness is similar or if the catchment is wet at key locations for water transport (Seyfried et al., 2009). These antecedent wetness conditions may reflect the ability of catchment storage to provide a “memory effect” of past inputs that can buffer short-term changes in inputs, but this memory varies among catchments and across years. Consequently, changes in snowfall fractions might not always affect stream discharge, especially in locations with a strong memory effect. Prevailing climatic conditions and subsurface storage capacity might also influence how precipitation is partitioned takes after it reaches the ground surface (Hammond et al., 2019), indicating that both the temporal and spatial distribution of SWI are important when considering how snowfall fractions affect seasonal to annual stream discharge generation.

Snowfall fractions may also influence the spatial distribution of SWI. In the semi-arid western US, rainfall magnitudes generally increase with elevation (Johnson and Hanson, 1995). In regions with large snowfall fractions, this general elevation-driven pattern can be overlain by impacts of wind-driven redistribution of snow, which is dependent on factors such as topography, aspect, wind speed and wind direction (Sturm, 2015; Tennant et al., 2017; Winstral and Marks, 2014; Trujillo et al., 2007). Hence, differences in the SWI distribution due to varying snow depths could be particularly substantial in areas where wind-driven redistribution of snowfall is significant. The primary controls (e.g., topography, aspect, elevation) on snow depth and snow water equivalent (SWE) are relatively consistent from year to year, so the interannual distribution of snow is usually spatially consistent (Parr et al., 2020; Sturm, 2015; Winstral and Marks, 2002). The effects of elevation and aspect on the spatial distribution of snow depth, and thus the potential for SWI as snowmelt, are well-studied in both high and mid-altitude mountains (e.g., Grünewald et al., 2014; López-Moreno and Stähli, 2008; Tennant et al., 2017). Studies on snow drifting in seasonally snow-covered areas (Mott et al., 2018), prairie and arctic environments (e.g., Fang and Pomeroy, 2009; Parr et al., 2020) and in the context of avalanches (e.g., Schweizer et al., 2003), have shown that snow drifts can strongly influence the spatial water balance. These studies also revealed that equator-facing slopes might only receive half as much SWI as snowmelt compared to snow drift areas (Flerchinger and Cooley, 2000; Marshall et al., 2019). In turn, water originating from snow drifts can locally control groundwater level fluctuations (Flerchinger et al., 1992), and contribute to streamflow

83 into the summer season (Chauvin et al., 2011; Hartman et al., 1999; Marks et al., 2002). Due to increases in temperature,
84 mountainous regions will receive less snow and more rain (Barnett et al., 2005; Stewart, 2009). This is concerning because
85 snowmelt is a primary source for water resources across the globe (Barnett et al., 2005; Marks et al., 1999; Somers and
86 McKenzie, 2020; Viviroli et al., 2007). The relative importance of spatial snowmelt patterns is expected to increase with
87 snowmelt magnitude, which is sensitive to snowfall fractions. Hence, quantifying spatial snowmelt patterns in areas that are
88 not seasonally snow-covered, and determining the importance of snow drifts for streamflow generation in these areas, could
89 be an important step in clarifying how stream discharge is affected by snowfall fractions.

90
91 One area where the snowfall fraction varies substantially from year to year is the rain-snow transition zone. On the scale of
92 the continental United States (US), a decrease in the fraction of precipitation falling as snow (snowfall fraction hereinafter) is
93 expected to decrease stream discharge (Berghuijs et al., 2014). However, lower snowfall fractions in much of the western
94 United States have not yet led to a significant decrease in annual discharge (McCabe et al., 2017). Nonetheless, both
95 observational data records (McCabe et al., 2017; Luce and Holden, 2009; Regonda et al., 2005) and future climate projections
96 (Naz et al., 2016; Leung et al., 2004; Milly and Dunne, 2020; Christensen et al., 2004) reveal earlier stream discharge peaks
97 in response to earlier snowmelt, and a decline in summer low flows across the semi-arid mountainous US. One emerging
98 question from these findings is how decreases in snowfall affect discharge in areas that already receive a mix of snow and rain.

99
100 The rain-snow transition zone is an elevation band within which the dominant phase of winter precipitation shifts between
101 snow and rain (Nayak et al., 2010), and is often characterized by a transient snowpack in (at least) parts of the defined area.
102 Multiple studies in the European Alps and the north-western United States/US have shown that snowfall fractions in lower and
103 mid-altitude mountains, where the rain-snow transition zone is located, are particularly vulnerable to increases in temperature
104 associated with climate change (Stewart, 2009). (e.g., Stewart, 2009). For example, the snowfall fraction in the Swiss Alps is
105 projected to decrease between 50% (at ~2000 m) to 90% (at ~1000 m) towards the end of the century (Beniston et al., 2003).
106 The current extent of the rain-snow transition zone covers about 9200 km² in the Pacific Northwest of the United States/US
107 alone (here defined as Oregon, Washington, Idaho and the western part of Montana; Nolin and Daly, 2006), and is expanding
108 and moving to higher elevations in response to climate change (Bavay et al., 2013; Nayak et al., 2010). This migration of the
109 transition zone can affect precipitation patterns as well as discharge generation and timing across mountain ranges, with notable
110 effects at the elevations surrounding the transition zone.

111
112
113 In addition to the climate expected decrease in snowfall fractions with climate change also has the potential to increase, annual
114 climate variations are expected to increase almost everywhere across the planet (Seager et al., 2012), affecting annual runoff
115 efficiency (Hedrick et al., 2020) (Hedrick et al., 2020) and likely also influencing stream discharge timing and magnitude. In
116 mid-elevation rain-snow transition zones the annual snowpack variability is already relatively large. For example, in the
117 Reynolds Creek Experimental Watershed (RCEW, in Idaho, US) the coefficient of variation (CV) of peak snow-water
118 equivalent (SWE) between 1964 and 2006 ranged from 0.28-0.37 for five high-elevation stations (2056-2162 m) and was 0.72
119 for a mid-elevation weather station at the rain-snow transition zone (1743 m, Nayak et al., 2010). This mid-elevation variability
120 suggests that year-to-year differences in snowfall at the rain-snow transition zone might already be substantial compared to
121 nearby catchments at higher elevations. This allows the investigation of catchment responses to snowfall variations using a
122 relatively short data record. One well-documented discharge response is that years in which catchments receive less snow have
123 earlier snow-driven discharge peaks (McCabe and Clark, 2005; Stewart et al., 2005) (McCabe and Clark, 2005; Stewart et al.,
124 2005). Earlier This is relevant because earlier spring snowmelt has been linked to an increased risk of wildfire for catchments
125 across the western US (Westerling et al., 2006), as well as to earlier and lower low-flows in late-summer and fall months
126 (Kormos et al., 2016). In some catchments and years, portions of the stream network might also dry, altering completely cease

127 to flow and this drying can alter the network's ecological and biogeochemical functioning (Datry et al., 2014). In mid-elevation
128 rain-snow transition zones, the annual snowpack variability is already relatively large. For example, in the Reynolds Creek
129 Experimental Watershed (RCEW, in Idaho, US) the coefficient of variation (CV) of peak snow-water equivalent (SWE)
130 between 1964 and 2006 ranged from 0.28-0.37 for five high-elevation stations (2056-2162 m) and was 0.72 for a mid-elevation
131 weather station at the rain-snow transition zone (1743 m, Nayak et al., 2010). This mid-elevation variability suggests that year-
132 to-year differences in snowfall at the rain-snow transition zone might already be substantial compared to nearby catchments at
133 higher elevations, and allows for the investigation of catchment hydrologic responses to snowfall variations using a relatively
134 short data record, especially in sites with a limited memory of past inputs. Using observations of hydro-climatically different
135 years (e.g., rainy vs. snowy) could reveal how discharge and stream drying at the rain-snow transition zone has responded to
136 past variations in water inputs, and thereby provide insight in how catchments other small (<10 km²) catchments with a similar
137 vegetation cover and precipitation regime might respond to future changes in rain/snow apportionments.

138
139 Annual or climate-driven variations in snowfall fractions might affect the spatial distribution of surface water inputs (SWI =
140 rainfall + snowmelt). In years that receive less snow, the spatial pattern of SWI could depend more on the spatial distribution
141 of rain, whereas the SWI pattern might reflect the distribution of the snowpack more strongly in years that receive more snow.
142 In the semi arid western US, rainfall magnitudes generally increase with elevation (Johnson and Hanson, 1995), whereas the
143 spatial distribution of the snowpack is dependent on elevation, aspect, and wind-driven redistribution of snow, among other
144 factors (Sturm, 2015; Tennant et al., 2017; Winstral and Marks, 2014; Trujillo et al., 2007). These primary controls on snow
145 depth and SWE are relatively consistent from year to year, so the interannual distribution of snow is usually spatially consistent
146 (Parr et al., 2020; Sturm, 2015; Winstral and Marks, 2002). The effects of elevation and aspect on the spatial distribution of
147 snow depth, and thus, SWI, are well studied in both high and mid-altitude mountains (e.g., Grünwald et al., 2014; López-
148 Moreno and Stähli, 2008; Tennant et al., 2017), and the seasonal spatial distribution of SWI has been quantified at the rain-
149 snow transition zone (Kormos et al., 2014). Snow drifting can also strongly impact the snowpack in the rain-snow transition
150 zone, but thus far, research on snow drifting has been focused mainly on seasonally snow-covered areas (Mott et al., 2018),
151 prairie and arctic environments (e.g., Fang and Pomeroy, 2009; Parr et al., 2020) or has been studied in the context of
152 avalanches (e.g., Schweizer et al., 2003). These studies have shown that snow drifts can strongly influence the spatial water
153 balance, that equator-facing slopes might only receive half as much SWI as areas that host snow drifts (Flerchinger and Cooley,
154 2000; Marshall et al., 2019), and that water originating from snow drifts can locally control groundwater level fluctuations
155 (Flerchinger et al., 1992), and contribute to streamflow into the summer season (Chauvin et al., 2011; Hartman et al., 1999;
156 Marks et al., 2002).

157
158 In addition to the spatial distribution of water inputs, the snowfall fraction also influences when SWI reaches the ground
159 surface. Snowpacks store water and release snowmelt later, whereas rain on bare ground enters the hydrologic system
160 instantaneously. After rainfall or snowmelt reaches the ground surface, it might become stream discharge, be stored in the soil,
161 recharge deeper groundwater, or be evaporated or transpired. Generally, water inputs from rain or snowmelt during periods
162 with high antecedent wetness and low evapotranspiration rates are more likely to recharge groundwater and generate discharge
163 (Jasechko et al., 2014; Molotch et al., 2009; Hammond et al., 2019). However, rain and snowmelt inputs might result in similar
164 runoff ratios (discharge/SWI) as long as the overall catchment wetness is similar or if the catchment is wet at key locations for
165 water transport (Seyfried et al., 2009). The precipitation phase might also affect other hydrological processes that control water
166 partitioning, for instance by inhibiting soil evaporation in areas that are snow-covered (Wang et al., 2013). Prevailing climatic
167 conditions and subsurface storage capacity might also influence which route precipitation takes after it reaches the ground
168 surface (Hammond et al., 2019), indicating that both the spatial and temporal distribution of SWI could affect if and when
169 water reaches the stream.

171 Thus, ~~our~~the overarching goal of this work is to improve our understanding of discharge ~~response~~responses to year-to-year
172 variations in precipitation phase and magnitude. We do this at the rain-snow transition zone - a region that experiences large
173 year-to-year variations in snowfall fractions, covers a significant part of the land surface and might extend to higher elevations
174 due to climate change. Specifically, we address the following research questions:

- 175
- 176 1. How does the spatial and temporal distribution of SWI at the rain-snow transition zone vary between particularly wet,
177 dry, rainy or snowy years?
- 178
- 179 2. How does stream discharge timing and amount respond to SWI in wet, dry, rainy or snowy years?
- 180 3. Are variations in stream discharge related to variations in yearly snowfall fractions?
- 181

182 Examining natural variation in snowfall fractions in the rain-snow transition zone contrasts with other research on snow-related
183 processes that focus on seasonally-snow covered catchments. While many studies of snowmelt runoff examine seasonal
184 responses at the landscape scale, here we focus on hourly responses at a fine spatial resolution. This allows us to investigate
185 the spatial distribution of the snowpack and snowmelt, as well as the phase of precipitation and the temporal distribution of
186 SWI. Furthermore, while SWE is frequently used as a summarizing variable for winter precipitation when comparing
187 precipitation to stream discharge, SWI is more directly related to the timing and amount of water resources, and might therefore
188 be an important variable to model in future work addressing similar questions. Lastly, we also compare stream discharge to
189 annual metrics of snowfall fraction and total precipitation to provide a finer-scale context for results from larger scale models
190 or estimations that rely on annual metrics.

191

192 2. Site description

193 ~~We focus our efforts in the~~Our study location is Johnston Draw ~~study area~~, a 1.8 km² headwater catchment at the Reynolds
194 Creek Experimental Watershed (RCEW) in Idaho, USA. Elevations range from 1497 to 1869 m a.s.l., and mean annual air
195 temperature and precipitation are 8.1 °C and 609 mm, respectively (2004-2014; Godsey et al., 2018). Previous research in
196 RCEW has shown that mid-elevation catchments (1404 and 1743 m a.s.l.) have seen an increase in minimum daily
197 temperatures (+0.57°C/decade), reduced snowfall (-32 mm/decade), and a decrease in streamflow ($-0.75 \times 10^6 \text{ m}^3$
198 mm/decade) over the 1965-2006 data record, while there was no change in total precipitation (Nayak et al., 2010; Seyfried et
199 ~~al., 2011~~)(Nayak et al., 2010; Seyfried et al., 2011). These streamflow trends are unlikely to be driven by increased plant water
200 use (caused by increased temperatures) because there is only a short time window (~weeks) in which plant leaf-out has occurred
201 and there is still sufficient soil water available in this water-limited environment (Seyfried et al., 2011). The catchment is
202 underlain by granite bedrock (79%), with some basalt (3%) and tuffs (18%) (Stephenson, 1970), and slightly deeper soils exist
203 on the north-facing slopes, although the difference is not significant (1.31 ± 0.56 m vs. 0.77 ± 0.34 m, respectively, p-value: 0.05;
204 Patton et al., 2019). Annual average soil water storage on the north-facing slopes is larger than on the south-facing slopes,
205 which is largely due to the difference in soil depth and a later start of vegetation growth compared to ~~the~~ south-facing slopes
206 (Godsey et al., 2018; Seyfried et al., in review)(Godsey et al., 2018; Seyfried et al., 2021). Snowberry (*Symphoricarpos*), big
207 and low sagebrush (*Artemisia tridentata* and *Artemisia arbuscula*), aspen (*Populus tremuloides*) groves and wheatgrass
208 (*Elymus trachycaulus*) characterize the north-facing slopes, whereas the south-facing slopes host *Elymus trachycaulus*,
209 *Artemisia arbuscula*, mountain mahogany (*Cercocarpus ledifolius*) and bitterbrush (*Purshia tridentate*) (Godsey et al., 2018).
210 Discharge at the catchment outlet is non-perennial, and the stream at the catchment outlet typically flows from early November
211 until mid-July (MacNeille et al., 2020)(MacNeille et al., 2020).

3. Methods

3.1 Hydrometeorological and discharge data

We used hourly hydrometeorological data recorded at eleven weather stations throughout the catchment (Fig. 1; Godsey et al., 2018). The stations are placed at 50-m elevation intervals on the north and south-facing slopes, and span a ~300 m elevation range (1508-1804 m a.s.l.; see Marks et al., 2013; Marks et al., 2013 for a detailed description). Observations started in 2002, although some stations were placed only in 2005 or 2010, and some were decommissioned in 2017 (see Godsey et al., 2018 for exact years). Air temperature, solar radiation, vapor pressure and snow depth were measured at hourly intervals at each of the stations, whereas additional measurements of wind speed, wind direction and precipitation were available at jdt125, jdt124, and jdt124b. The snow depth time series were processed to remove gaps and unreliable measurements during storms and smoothed over an 8-h window in most cases, and a 40-h window under specific circumstances (Godsey et al., 2018). Stream discharge data (Godsey et al., 2018) were obtained with a stage recorder using a drop box weir at the watershed outlet (Pierson et al., 2000). Stage height was converted to discharge using a stage-height-discharge relationship rating curve (Pierson and Cram, 1998), and discharge was frequently measured by hand to ensure high data quality (Pierson et al., 2000).

3.2 Remotely sensed observations

To characterize the spatial distribution of snow depth, a 1-m resolution snow depth product was calculated as the difference between a snow-off LiDAR flight (10-18 November 2007; Shrestha and Glenn, 2016) and a snow-on LiDAR flight (18 March 2009, around the time of peak accumulation), hereafter referred to as lidar snow depth. Typical vertical accuracies for lidar surveys are ~10 cm (Deems et al., 2013). We assumed that uncertainties in both lidar surveys were uncorrelated, resulting in an overall uncertainty of ~14 cm for lidar snow depth (summation in quadrature of uncertainties associated with each survey). All pixels that yielded a negative snow depth were excluded. The lidar snow depths were higher than the weather station snow depths, but this pattern was consistent across the catchment resulting in a strong linear relation between the two individual sets of snow depth measurements ($R^2 = 0.88$, Supplemental Fig. S1).

Because we had only one lidar observation was available near peak snow accumulation, we also characterized snow presence throughout the season by mapping the snow-covered area (SCA) using satellite-derived surface reflectance at 3-m resolution, which is available starting in 2016 (4-band PlanetScope Scene; Planet Team, 2018). This high-resolution imagery was critical for our analysis because snow drifts in the rain-snow transition are relatively small in extent. Although no high-resolution satellite imagery was available for years that exhibited the key characteristics we sought to study (e.g., rainy, snowy, wet or dry; see section 3.3), so we focused on the most recent snow-covered period for which streamflow data and Planet imagery were available (1 November 2018 until 31 May 2019) to assess snow coverage. This targeted year was warmer than the year for which the lidar observations were available (mean annual air temperature: 8.0°C compared to 6.7°C in 2009), which may have resulted in earlier peak streamflow, melt-out date, and dry-out date for the stream. We manually selected all available images in which the entire watershed was captured and for which snow was visually recognizable, then removed all images for which clouds significantly covered the watershed, resulting in 41 usable images. The information from all four spectral bands was then condensed to one layer using a principal component analysis ('RSToolbox' package in R). We used the Maximum Likelihood Classification tool in ArcGIS (Esri Inc., 2020) to identify the SCA, after manually training the tool by selecting areas with and without snow cover (average mean of 26895 pixels per class; median: 9019), visually aided by the original satellite imagery. Obtaining training data was most challenging during periods in which almost the entire area was snow-free or snow-covered, for densely vegetated areas, and when part of the catchment was shaded. To overcome the latter, we classified "snow-free", "snow-covered", and "shaded snow" in heavily shaded images, and afterwards merged "snow-

Formatted: Font color: Auto

covered” and “shaded snow”. The mean confidence for all classifications is shown in [Supplemental Fig. S2](#). Our method differs from other satellite-derived snow products that combine both visible and infrared light, but yielded a higher resolution data product (3-m resolution vs. 30-m for Landsat-8 or 500-m for MODIS) that was necessary to capture the snow drifts in the rain-snow transition zone.

We also used the surface reflectance imagery to determine the melt-out date of the snowpack for all years in which satellite and discharge observations were available (2016-2019). This was done by manually reviewing all available images and visually determining when all snow had melted. Given the high visiting frequency and limited cloudiness in early summer, we estimate [that](#) an error of ~2 days is appropriate for these melt-out dates.

3.3 Spatially distributed snowpack modelling

We used the Automated Water Supply Model (AWSM; Havens et al., 2020) to obtain ~~a~~ spatially continuous ~~estimates~~ estimates of the distribution and phase of precipitation, snowpack characteristics and surface water inputs (SWI). The two major components of AWSM are the Spatial Modeling for Resources Framework (SMRF; Havens et al., 2017) and iSnobal (Marks et al., 1999). ~~iSnobal is~~ SMRF was used to spatially distribute precipitation and all other weather variables (air temperature, solar radiation, vapor pressure, precipitation, wind speed and wind direction) along an elevation gradient using the hourly measurements from the weather stations. We included precipitation measurements from two stations within the basin (jdt125 and jdt124b) and two stations outside of the basin (jd144 and jd153, Fig. 1) to capture the elevation gradient. ~~Precipitation at the wind-exposed site, jdt124, was excluded because of precipitation undercatch issues. The interpolated vapor pressure and temperature fields were then used within SMRF to calculate the dew point, and further distinguish which fraction of precipitation fell as rain and/or snow. The output from SMRF was then used to force iSnobal, a physically-based, two-layer snowpack model that accounts for precipitation advection from rain and snow (Marks et al., 1999). We used SMRF to spatially distribute precipitation and all other weather variables (air temperature, solar radiation, vapor pressure, precipitation, wind speed and wind direction) along an elevation gradient using the hourly measurements from the weather stations. We included precipitation measurements from two stations within the basin (jdt125 and jdt124b) and two stations outside of the basin (jd144 and jd153, Fig. 1) to capture the elevation gradient. Precipitation at wind-exposed site jdt124 was excluded because of precipitation undercatch issues. The interpolated vapor pressure and temperature fields were then used within SMRF to calculate the dew point, and further distinguish which fraction of precipitation falls as rain and/or snow.~~

The model was run at a 10-m resolution for five water years, namely, 2005, 2009, 2010, 2011 and 2014. We selected 2009 because the snow depth lidar survey was available in this year, and 2005, 2010, 2011 and 2014 because they ~~provide a~~ provide a representation of rainy, snowy, dry and wet conditions, respectively (Table 1). ~~We focus on the latter four years in the results and discussion of this manuscript but evaluate the model performance for all~~ We focus on the latter four years in the results and discussion of this manuscript, but evaluate the model performance for all hydroclimatically different. 2005 was rainy (snowfall fraction: 63% of the 2004-2014 mean and 23% of 2005 total precipitation) whereas 2010 was snowy (snowfall fraction: 155% of 2004-2014 mean and 57% of 2010 total precipitation). 2014 was dry (precipitation: 86% of 2004-2014 mean) and 2011 was wet (precipitation: 132%) (Table 1, Supplemental Table S3 and Fig. S4) with snowfall fractions of 41% and 30% of the total precipitation for each year, respectively. The work was limited to four years because we aimed to focus on differences in the distribution of SWI and stream discharge for years that had different snowfall fractions and total precipitation magnitudes. Therefore, these strongly contrasting years were selected from 11 potential years of record (Godsey et al., 2018). ~~Towards the end of the 2004-2014 period, more stations were deployed, yielding additional observations to force the model with meteorological inputs and validate the model output of snow thickness, so if conditions were similar, we selected later years within this period. We focus on the four hydroclimatically distinct years in the results and discussion of this manuscript, but evaluate the model performance for all five years.~~

291 In order to represent the spatial variability in snowfall and the effects of wind redistribution of snow, we use the precipitation
292 rescaling approach proposed by Vögeli et al. (2016) that implicitly captures the spatial heterogeneity induced by these
293 processes using distributed snow depth information (e.g., from lidar or structure from motion (SfM)). This methodology can
294 be used to rescale the precipitation falling as snow to reproduce the observed snow distribution patterns while conserving the
295 initial precipitation mass estimation. Given the inter- and intra-annual consistency of spatial patterns of snow distribution
296 (Pflug and Lundquist, 2020; Schirmer et al., 2011; Sturm and Wagener, 2010)(Pflug and Lundquist, 2020; Schirmer et al.,
297 2011; Sturm and Wagener, 2010), Trujillo et al. (2019, manuscript in preparation)Trujillo et al. (2019) has been extending the
298 original implementation to utilize historical snow distribution information to other years in the iSnoBal model. Following these
299 successful implementations, we used the spatial distribution of snow depth from the 2009 survey around peak snow
300 accumulation to inform the snowfall rescaling to all years in the study period. Although using the 2009 survey to rescale
301 snowfall in other years might have induced some uncertainty, this uncertainty is likely to be small given verification of the
302 intra-annual/interannual consistency in the snow distribution patterns, which was verified in this catchment by comparing the
303 lidar snow depth and the satellite imagery indicated that this uncertainty is likely to be small.

304 3.4 SWI

305 ~~One of the model outputs from iSnoBal is 'surface water inputs' (SWI), which represents snowmelt from the bottom of the~~
306 ~~snowpack, rain on bare ground, or rain percolating through the snowpack. iSnoBal is limited to surface~~
307 ~~One of the model outputs~~
308 ~~from iSnoBal is 'surface water input' (SWI), which represents snowmelt from the bottom of the snowpack, rain on snow-free~~
309 ~~ground, or rain percolating through the snowpack. Rainfall is directly counted as SWI when it falls over snow-free ground,~~
310 ~~and it is included in the energy and water balances when it falls onto the snowpack. To calculate snowmelt, iSnoBal solves~~
311 ~~each component of the energy balance equation for each model time step using the best available estimations of forcing inputs.~~
312 ~~Melt occurs in a pixel when the accumulated input energy is greater than the energy deficit (i.e. cold content) of the snowpack.~~
313 ~~If the accumulated energy input is smaller than the energy deficit, the sum of current hour melt and previous hour liquid water~~
314 ~~content will be carried over into the next hour. If that hour's input energy conditions are negative, the liquid mass is refrozen~~
315 ~~into the column. Sublimation and evaporation of liquid water from the snow surface and condensation of liquid water onto the~~
316 ~~snow surface is computed as a model output term, though these quantities were not considered here. Canopy interception must~~
317 ~~be handled a priori when developing the model forcing input, and it was also not considered here. Although not accounting for~~
318 ~~the latter introduces some uncertainty, we expect this to be small with the shrub and grass vegetation types in Johnston Draw.~~
319 ~~Lastly, iSnoBal is limited to snow processes only, which means that SWI 'exits' the modelling domain. In reality, SWI might~~
320 ~~travel to the stream as surface or subsurface runoff, could be stored in the soil until it evaporates or is transpired, or could~~
321 ~~recharge deeper groundwater storages. The route that SWI takes depends on the overall catchment wetness as well as the local~~
322 ~~energy balance (e.g., incoming radiation) and vegetation activity. In this manuscript, we computed SWI for each pixel and~~
323 ~~time step and assumed that all SWI generated in simulated snow-free pixels was rain and that all SWI generated in simulated~~
~~snow-covered pixels was snowmelt.~~

324 3.5 Model evaluation

325 Model results were evaluated in two ways. First, the simulated snow depths were compared to lidar snow depths covering the
326 entire basin on March 18, 2009; and second, the temporal variation of the simulated snow depths were compared to snow
327 depths measured at each of the weather stations for all simulated years. The latter comparison was done using model results
328 from a 30-m x 30-m area surrounding each station; this is equivalent to 3x3 grid cells because the model was run at a 10-m
329 resolution. We computed the Root Mean Square Error (RMSE) and Nash-Sutcliffe Efficiency (NSE; Nash and Sutcliffe, 1970)

330 for the observed versus simulated snow depths, as well as the NSE for the normalized observed versus normalized simulated
331 snow depths (NSE_{norm}). NSE_{norm} reflects the ability of the model to reproduce the dynamic behaviour of the snowpack.

332 3.6 Comparison with discharge

333 The phase and magnitude of precipitation and the magnitude and temporal distribution of SWI were compared to annual
334 discharge and the stream dry-out date. The stream dry-out date is the day when the stream first ceased to flow at the catchment
335 outlet. For comparisons across seasons, we defined winter as December, January and February; spring as March, April and
336 May; summer as June, July and August, and fall as September, October and November. To compare SWI with the dry-out
337 date, we also calculated how much SWI occurred during the water year before the stream dried. No delays were considered
338 when comparing SWI to discharge (e.g., discharge as a fraction of SWI in January results from dividing discharge in January
339 by SWI in January). Discharge metrics were also compared to the flashiness of SWI inputs, which was calculated as the sum
340 of the difference in total SWI from day to day, divided by the sum of SWI (also known as the Richards-Baker Flashiness Index;
341 Baker et al., 2004). Further metrics included the fraction of time that more than half of the catchment was snow-covered and
342 the melt-rate between 40% snow-coverage in the catchment and the date at which the catchment was snow-free. A threshold
343 of 40% snow-coverage was chosen because this resulted in an approximately linear melt-rate for all years.

344 **4. Results**

345 **4.1 Snow depth observations**

346 The lidar snow depth ranged from 0 to 5.3 m on the date of acquisition (18 March 2009), which was near peak snow cover
347 (median: 0.4 m; CV: 0.91; Fig. 2a). The south-facing slopes had little to no snow cover (mean: 0.3 m), whereas the north-
348 facing slopes were covered with 0.7 m of snow on average. For the years studied here, during the approximate duration of the
349 snowy season between 15 Nov and 15 Apr, the average snow depth for all north-facing stations was more than five times that
350 of the average snow depth at south-facing stations (0.20.2 vs. 3.7 ~~m~~0.04 m, respectively), and the snowpack lasted almost 90
351 days longer on average (132 vs. 43 days, respectively). ~~Although weather~~Weather stations on north-facing slopes and at higher
352 elevations generally had deeper snowpacks and were snow-covered longer than sites on the south-facing slopes or at lower
353 elevations (data not shown), this pattern was masked by the effects of other processes (Godsey et al., 2018). The snowpack
354 distribution was also affected by wind-driven redistribution of snow. For instance, snow depths at jdt2 (north-facing) and jdt3b
355 (south-facing) were consistently lower than at the weather stations directly below them in elevation (jdt1 and jdt2b,
356 respectively). Large snow drifts formed in some western parts of the watershed, up to a maximum depth of 5.3 m
357 (90th percentile of all snow depths = 1.2 m, Fig. 2a). Wind-driven redistribution of the snow in Johnston Draw is facilitated by
358 a relatively consistent southwestern wind direction (average during storms: 225°), and high wind speeds (average during storms
359 at wind-exposed station jdt124: 6.7 m s⁻¹; Godsey et al., 2018Supplemental Fig. S5).

360 **4.2 Model performance in space and over time**

361 Simulated snow depths on the day of the lidar survey agreed well with the lidar snow depth (r^2 : 0.88, Fig. 2a-c). The residual
362 snow depths (lidar – simulation) were approximately normally distributed, with a mean of 0.2 m (see Supplement
363 S3Supplemental Fig. S6 for a histogram and QQ-Q plot). The largest differences (maximum difference: 1.1 m) between the
364 simulated and measured snowpack were for isolated 10 m pixels on both the north- and south-facing slopes (Fig. 2e2a-c). The
365 spatial pattern of the lidar snow depth also agreed well with the spatial patterns of snow-covered area (Fig. 2a,d), and there
366 was a strong agreement between the simulated snow-covered area for 2009 (Fig. 2e) and the snow-covered area determined

Formatted: Font color: Auto

Formatted: Font color: Auto

Formatted: Font color: Auto

Formatted: Font color: Auto

367 from satellite imagery for 2019 (Fig. 2d). This, including the modelled duration of snow cover and the number of satellite
368 images in which snow-covered areas were observed. The largest discrepancy between the simulated and imagery-based snow
369 duration was in the scour zone west of the snow drifts, where the model underestimated snow duration. Nonetheless, the
370 consistent locations of the snow drifts between 2009 and 2019 indicates that the model captured the spatial distribution of the
371 snowpack as well as the differential melt-out patterns, and that the location of the snow drifts was consistent between 2009
372 and 2019.

374 The median NSE for the hourly simulated snow depths compared to observations at the weather stations ranged from 0.22
375 (wet 2011) to 0.86 (snowy 2010) for all modelled years and weather stations, with RMSE ranging from 0.8008 to 9.7 cm 0.097
376 m (Table 2, see Supplement S4 Supplemental Fig. S7 for time series of all simulated and observed snow depths). RMSE was
377 equal to or lower than 40 cm 0.1 m for all years, with the year in which the NSE performance was lowest (wet 2011) having
378 an RMSE of 4.6 cm. There were no weather stations for which the model performed consistently poor or well, with both high
379 and low NSE values at each of the stations (e.g., range NSE at jdt4: -9.60 to 0.91 and jdt1: 0.01 to 0.83) 0.046 m. The temporal
380 variation of the snowpack at each of the weather stations was well-captured by the model; the median NSE for the normalized
381 snowpack depths (NSE_{norm}) ranged from 0.65 to 0.94 (median: 0.75), although there were some sites and years with low NSE
382 (Table 2). This indicates that the overall patterns of snow accumulation and melt were captured by the model Both high and
383 low NSE values are observed at nearly all of the stations (e.g., range NSE at jdt4: -9.60 to 0.91 and jdt1: 0.01 to 0.83) with
384 lower values at some sites in 2011. Possible explanations for the relatively low performance at the remaining sites are discussed
385 further in section 5.3. Despite the low performances for some years and locations, the normalized snow depths were largely
386 acceptable (35 out of 40 year/location-combinations had NSE_{norm} value above 0.5; Table 2). The generally strong performance
387 lends confidence that the simulation of ablation and accumulation processes in the model is reasonable and implies that the
388 temporal distribution of snow-covered area (SCA) and surface water inputs (SWI) simulated by the model are reliable.

389 4.3 Spatial and temporal pattern of surface water inputs (SWI)

390 The spatial pattern of SWI was similar for all years, with the highest SWI occurring in areas hosting the snow drifts (maximum
391 SWI (SWI_{max}): 3892 mm; 98th percentile of SWI (SWI₉₈): 1235 mm, both in wet 2011; Fig. 3, Table 1). Annual SWI across
392 the rest of the catchment varied less, with north-facing slopes receiving 45 to 127 mm more SWI than south-facing slopes
393 (values for rainy 2005 and snowy 2010, respectively; Table 1). Areas hosting snow drifts Snow drift locations received 1.7 to
394 2.7 times more SWI than the catchment average (ratio SWI₉₈/SWI_{avg}). Summarizing SWI by aspect (see polar diagrams in Fig.
395 3) revealed the highest SWI on northeast-facing slopes and roughly equal annual SWI for all other aspects. Differences between
396 the northeast-facing slopes and other parts of the catchment were largest in snowy 2010 (ratio of major/minor axis of polar
397 plot: 1.29), and smallest in rainy 2005 and dry 2014 (ratio: 1.13 and 1.17, respectively).

398 Weekly sums of SWI ranged from 0 to ~75 mm in all years (Fig. 4). Summer most frequently had weeks without SWI
399 generation, whereas the highest weekly SWI occurred with simultaneous rainfall and snowmelt (i.e., rain-on-snow events, such
400 as for instance the one visible in February 2014, Fig. 4d). However, large rainfall events without snowfall or snow cover in
401 spring of rainy 2005 (weekly SWI: ~75 mm) and in fall of wet 2011 (weekly SWI: ~50 mm; grey peaks in Fig. 4a and c) also
402 generated high SWI. In 2011, the majority of SWI was generated in winter and spring (47% between December and May, see
403 inset in Fig. 4c) whereas in dry 2014 most SWI was generated in winter (54% between December and February, Fig. 4d). In
404 2005 and 2010, most SWI was generated in spring (March-May 32% and 46%, respectively). Although similar Similar amounts
405 of SWI occurred in spring in 2005 and 2010 (339 and 388 mm, respectively); however, in 2005, 93% came from rain, whereas
406 in 2010, only 35% came from rain. As a result, average Average daily spring SWI rates were higher in snowy 2010 than in
407 rainy 2005 (mean spring SWI rate March-May: 3.7 mm d⁻¹ in 2010 vs. 2.9 mm d⁻¹ in 2005). Overall, variations in weekly and
408

409 daily SWI rates were lower in snowy 2010 (CV daily SWI: 1.71) than in all other years (2.50 in 2005, 2.14 in 2011, and 2.65
410 in 2014).

411 4.4 Stream discharge

412 Streamflow was least responsive to SWI at the beginning of each water year (Fig. 5). For instance, in 2005 and 2010, 174 and
413 108 mm of SWI occurred before February 1st (31% and 20% of annual SWI), whereas discharge amounted to only 7% and 1%
414 of its yearly total during that same period. Similarly, 82 mm of SWI in October 2011 resulted in less than 1 mm discharge,
415 whereas ~~roughly 30% 180 mm~~ of SWI ~~left the catchment via the stream in the following period (Nov-Jan SWI: 180 led to~~
416 ~~62 mm, of discharge: 62 mm). After the wet up period, SWI, SWI generally~~ resulted in most discharge when SWI rates were
417 high, such as during a 3-day rain-on-snow event in February 2014 (SWI: 75 mm, discharge: 29 mm) or during spring snowmelt
418 in April 2011 (SWI: 108 mm, discharge: 102 mm). Such individual precipitation events had a strong influence on the annual
419 runoff efficiency. For instance, 2014 had a slightly higher runoff efficiency (0.16) than 2005 (0.11) and 2009 (0.14), mostly
420 due to the high runoff generation during one rain-on-snow event (29 mm, 36% of yearly discharge).

421
422 Annual discharge was highest in 2011 (307 mm, 43% of SWI) and lowest in 2005 (62 mm, 11% of SWI). Despite similar SWI
423 ~~inputs~~ in 2005 and 2010 (SWI_{avg}: 553 and 557 mm, respectively, Table 1), snowy 2010 had nearly twice as much annual
424 discharge as rainy 2005 (117 mm; or 21% of SWI vs. 62 mm or 11% of SWI, respectively). Apart from these two years, there
425 was no relation between annual discharge and the annual snowfall fraction (Fig. 6c), nor between annual discharge and the
426 amount of SWI ~~coming in as rain produced by rainfall~~ or ~~snow snowmelt~~ in different seasons (winter, spring, summer, or any
427 combination of these periods). By considering additional years (for which SWI was not simulated), we found that annual
428 discharge was positively related to the amount of precipitation recorded at the lowest elevation precipitation station (jdt125,
429 $r^2=0.8083$, Fig. 6a). Annual discharge was slightly higher for years that were preceded by a year that received above average
430 annual precipitation (see Supplement S6 Supplemental Fig. S8), but the correlation coefficient decreased when including the
431 precipitation totals recorded in the preceding year (e.g., annual discharge vs. precipitation in the same year + 0.5 times
432 precipitation previous year, ~~S6~~). This indicates that any memory effect is likely to be small in this catchment. ~~This indicates~~
433 ~~that any memory effect is likely to be small in this catchment.~~ Frequent stream drying (16 out of 18 years between 2003 and
434 2020, data not shown, the stream did not cease flow in 2006 and 2011) and the high potential evaporation rates in this semi-
435 arid, high desert system (evapotranspiration accounts for nearly 90% of precipitation in the nearby Upper Sheep Creek
436 catchment; Flerchinger and Cooley, 2000) also suggest that any water in the shallow, 'active' subsurface storage is likely
437 limited, and that any memory effect, if present, is perhaps constrained to deeper subsurface water storages.

438
439 ~~Except for wet 2011, the Comparison of annual runoff efficiency (discharge/SWI) was higher for years that had a lower average~~
440 ~~weekly SWI rate (annual SWI/number of weeks in which SWI was generated). Although and the stream dry-out date to metrics~~
441 ~~describing the phase and magnitude of precipitation, the temporal distribution of SWI is affected by the phase of precipitation~~
442 ~~(Fig. 4), average weekly SWI rates and key characteristics of the snowpack highlighted the importance of the magnitude and~~
443 ~~timing of SWI (Fig. 7). Significant relationships with annual discharge were not related to the found for annual precipitation~~
444 ~~(Fig. 6a) and the sums of precipitation and snowfall in spring (Fig. 7 and Supplemental Fig. S9). The dry-out date of the stream~~
445 ~~was significantly correlated to annual precipitation, the sum of winter and spring precipitation and spring snowfall, spring~~
446 ~~precipitation as a fraction (r^2 of SWI, 0.06). Individual precipitation events also had a strong influence on the annual runoff~~
447 ~~efficiency. For instance, dry 2014 had a higher runoff efficiency (0.16) than 2005 (0.11) and 2009 (0.14), but this was mostly~~
448 ~~due to the high runoff generation during one rain-on-snow event (29 mm, 36% of yearly discharge).~~

450 Stream drying occurred in each of the five years except 2011 (Table 1, Fig. 5). The stream dried earliest in 2014 (13 July), and
451 in late August in 2009, 2005 and 2010 (Table 1). For the five years studied here, the stream dry-out date (the first day at which
452 discharge equals zero) was later for years receiving more SWI (r^2 : 0.84), and for years that had a later melt-out date (date at
453 which all snow had melted; r^2 : 0.77 for all coloured points in Fig. 6b). When considering the melt-out dates for four additional
454 years based on planet-lab satellite observations (2016–2019, section 3.2), we found that date of the snowpack, and the sum of
455 SWI before the dry-out date was later in years when snow persisted longer (r^2 : 0.54 for all points in Fig. 6b). There was no
456 relation (Fig. 7 and Supplemental Fig. S9). No significant correlation was found between the annual winter and spring snowfall
457 fraction and annual discharge and the stream dry-out date (Fig. 6d, 7).

459 5. Discussion

460 5.1 Spatial variability in SWI

461 Snow drifting and aspect-driven differences in snow dynamics caused a strong variability in the spatial pattern of the snowpack
462 (Fig. 2a) and SWI (Fig. 3). We found that the spatial pattern in simulated SWI was similar across all years, with snow drifts
463 receiving up to seven times more SWI than the catchment average (SWI_{max}/SWI_{avg} in 2010, Table 1). Even in rainy 2005, SWI
464 was more than 3.5 times higher in the snow drifts (SWI_{max} : 2005 mm) compared to the catchment average (SWI_{avg} : 573 mm,
465 Table 1). In our modelling routine, the spatial consistency between years is pre-determined by the snowfall rescaling (see
466 section 3.3), but this likely also reflects real-world conditions, as suggested by the spatial agreement between the independently
467 collected satellite imagery and lidar snow depths suggests (Fig. 2). Most importantly, the nearly four-fold variation in SWI
468 over less than a kilometre distance is equivalent to the average precipitation difference between most of Reynolds Creek and
469 the peaks of the Cascade Mountains in Oregon hundreds of kilometres away, or equivalently, shifting from a semi-arid steppe
470 to coastal mountain snowpacks, and snowpack. This difference directly affects water-limited processes such as weathering or
471 the plant species distribution. One local example of In Johnston Draw, this are the is clearly visible: aspen stands which are
472 uniquely located directly below the snow drifts (Kretschun et al., 2020), while sagebrush is predominant in the rest of the
473 catchment (Kretschun et al., 2020) and sagebrush dominates the rest of the catchment. Because snow drifts drive the spatial
474 pattern of SWI, it is crucial to quantify wind-driven redistribution processes as well as capture aspect and elevation-driven
475 processes, even at the rain-snow transition zone.

476
477 Snow drifts delivered 4.2% (2005) to 7.2% (2010) of the basin-total annual SWI on just ~2% of the land surface, and snow in
478 drifts persisted longer, compared to non-drift areas, into the spring season (Fig. 3d, 2d-e). Previous work in the seasonally snow-
479 covered Reynolds Mountain East catchment, showed that snow drifts indeed hold a large fraction of total catchment snow
480 water equivalent (SWE), with 50% of total SWE on just 31% of the catchment area (Marks et al., 2002), and SWI varying
481 strongly in space, ranging from 150 to 1100 mm for individual grid cells (10 – 20 m) in the relatively dry water year 2003
482 (Seyfried et al., 2009). Snow drifts in Johnston Draw were shallower (up to 5 m in 2009) and covered a smaller portion of
483 the area (~2%) than in the higher elevation Reynolds Mountain East catchment, but are proportionally even more important in
484 the rain-snow transition zone by holding up to 15% of SWE during peak SWE in snowy 2010 and 25% in rainy 2005.
485 Water originating from snow drifts has been shown to locally control groundwater level fluctuations (Flerchinger et al., 1992),
486 and contribute to streamflow into the summer season (Chauvin et al., 2011; Hartman et al., 1999; Marks et al., 2002). For
487 instance, in the Upper Sheep Creek watershed, also in RCEW, Chauvin et al. (2011) showed that the lowest stream discharge
488 was recorded for the year in which snow drifts were least prominent. In Johnston Draw, the stream dry-out date was positively
489 correlated with the drift melt-out date (Fig. 6b), suggesting that isolated snow patches are also here important for sustaining
490 streamflow. These results do not reveal the mechanism or influence of the specific drift location since neither subsurface flow
491 nor streamflow generation processes were measured or simulated. Nonetheless, observations of snow drifts from high-

492 resolution satellite imagery are largely consistent with model simulations of SCA (Fig. 2) and 6) and are easily obtained from
493 high-resolution imagery. This suggests that satellite observations might thus may be an alternative information source used to
494 predict stream drying in drift-influenced watersheds.

495 5.2 Temporal variability in SWI and discharge response

496 We found that the majority of SWI occurred in winter and spring, and that catchment-average SWI was more uniform in time
497 in snowy 2010 than in the other years (CV of daily SWI_i in 2010: 1.7; other years: 2.14 – 2.65). We hypothesize that the
498 steadier water inputs in that year the snowmelt period might explain why annual discharge in snowy 2010 was double that of
499 rainy 2005 despite similar precipitation total SWI. More stable water inputs from snowmelt rather than flashy water inputs from
500 rain could have led to wetter soils and higher soil conductivity rates, allowing more water to pass through the subsurface
501 towards the stream or towards deeper storages storage (Hammond et al., 2019). Previous work in the nearby Dry Creek
502 Experimental Watershed (Idaho) showed that water stored in the soil dries out approximately ten days after snowmelt
503 (McNamara et al., 2005). For the years on record here, streamflow was sustained for a minimum of 59 days after the melt-out
504 date (Table 1), while even though SWI during this period was is generally low after June each year (Fig. 4). This underscores
505 that it is indeed likely that deeper flow paths contributed contribute to the stream in the early summer. This is also consistent
506 with stream discharge being nearly unresponsive to SWI during the dry catchment conditions in the beginning of each water
507 year (Fig. 5). During fall, subsurface water storage across the catchment is low, and any SWI during this period thus likely
508 results in recharge rather than stream discharge (Seyfried et al., in review). Alternatively, SWI during early fall might be used
509 to satisfy evaporative demands. In any case or evaporation rather than stream discharge (Seyfried et al., 2021). Air temperature
510 also has a small effect on the runoff efficiency, particularly in the summer season. The runoff efficiency, calculated as summer
511 discharge divided by summer precipitation for the 2004-2014 record, was significantly correlated to summer air temperatures
512 ($r^2=-0.54$, p value=0.08, Supplemental Fig. S10) whereas this relationship was insignificant on the annual scale ($r^2=-0.43$, p -
513 value=0.217; Supplemental Fig. S11). This suggests that evapotranspiration, which is directly affected by the ambient air
514 temperature, has some influence on runoff efficiency, despite the catchment being an overall water-limited environment. In
515 winter, higher temperatures result in higher runoff efficiencies ($r^2=0.48$, p -value=0.131, Supplemental Fig. S10), which is
516 likely due to faster melt-out and more saturated soils, as described above. However, further simulations are required to fully
517 understand how precipitation amounts, timing and location interact with subsurface water storage to control stream discharge.
518

519 In contrast to our hypothesis and what has been suggested in the literature (e.g., based on the comparison of 420 catchments
520 in the continental US using the Budyko framework, Berghuijs et al., 2014), neither annual discharge nor the stream dry out-date
521 were correlated with snowfall fraction (Fig. 6, 7). Instead, annual discharge and the stream dry-out date were more correlated
522 with total precipitation and the snowpack melt-out date were positively related to annual discharge and the stream dry-out date.
523 This highlights the importance of the temporal distribution of SWI, which is not captured in an annual value for snowfall
524 fraction. The temporal distribution of SWI might be less important for predicting stream discharge and cessation in more humid
525 catchments in which precipitation is more evenly distributed over the year and/or in which more precipitation events occur, or
526 in larger catchments, such as those considered in Berghuijs et al., (2014; range catchment areas: 67-10,329 km²). We found
527 that individual precipitation events can also heavily influence the yearly runoff efficiency, as described for 2014 (section 4.4).
528 As such, considering inter-annual variability and rainfall or snowmelt events is an important addition to annual average values,
529 when investigating how precipitation affects discharge in semi-arid regions.
530

531 Bilish et al. (2020) similarly found that streamflow was not correlated to the snowfall fraction for a small catchment with an
532 ephemeral snowpack in the Australian Alps. They attributed this to the frequent occurrence of mid-winter snowmelt; the
533 snowpack melted out several times each year, independent of the annual snowfall fraction, and the snowpack thus did not store

Formatted: Font color: Auto

534 a significant amount of water. Field observations at Dry Creek, a nearby semi-arid catchment that includes a rain-dominated
535 and a snow-dominated area, also suggested that the snowfall fraction was not related to annual discharge for a small sub-
536 catchment at the rain-snow transition zone (Treeline sub-catchment, 0.015 km²), but a relation did exist snowfall fraction was
537 correlated with annual discharge when considering the entire Dry Creek catchment (28 km², J. McNamara, personal
538 communication). Another study at Dry Creek suggested that the snowfall fraction is less important than spring precipitation
539 for sustaining to satisfy evaporative demands of upland ecosystems (McNamara et al., 2005), emphasizing the importance of
540 the temporal distribution of SWI for other semi-arid catchments. For the years studied here, we did not find a relation between
541 stream drying and spring precipitation, but our findings do corroborate found that streamflow is more sensitive to spring
542 precipitation and total precipitation than to, but that the snowfall fraction did not significantly affect stream discharge (Fig. 6,
543 7).

544 5.3 Limitations and opportunities

545 Though the model adequately reproduced the spatial snowpack patterns and dynamics (Fig. 3 and Table 2), temporal variations
546 in the snow depths (i.e., melt and accumulation) recorded at the weather station locations were simulated better than the
547 absolute snow depths. We To investigate why simulations of snow depths were poor for some stations and years, we calculated
548 the average and precipitation-weighted average wind directions, wind speeds and snow densities for all events during which
549 the snowfall fraction was higher than 0.2 (i.e., 20%; see Supplemental Table S12 and Fig. S13) from the station data. Although
550 wind speed and directions were generally consistent (Supplemental Fig. S13), in 2011, the combination of higher snow
551 densities (stronger cohesion of snow particles; 122 kg m⁻²) and lower wind speeds (less energy for transport; 5.7 m s⁻¹)
552 compared to 2009 (102 kg m⁻² and 6.5 m s⁻¹, respectively, precipitation-weighted averages in Table S12) might have led to
553 less wind redistribution of snow in that year and correspondingly resulted in underpredictions of snow depths at north-facing
554 and high-elevation sites in 2011 (jdt3, jdt4, jdt5 and jdt124b). Since NSE values are based on squared errors, the divergence
555 between the simulated and observed snow depths impacted the model performance more severely in 2011 than in years with
556 shallower snowpacks (i.e., 2005 and 2014). The snowpack density, wind speed and wind direction values in 2005 diverged
557 most from 2009, from which the lidar observations were used, but nonetheless had a relatively high performance (NSE: 0.83),
558 possibly because there was data from only one station available for validation.

559 In addition to the uncertainty in the spatial redistribution of snow depending on wind speeds, wind direction and snow densities,
560 we suggest three additional reasons for the differences between simulated and observed snow depths. First, there was
561 uncertainty in the precipitation measurements and the spatial distribution thereof. Precipitation the varying performance at
562 jdt125 might be related to inaccuracies in calculating the phase of precipitation, which would most strongly affect lower
563 elevations at which the phase shifts more often from rain to snow. Any uncertainty in the magnitude or phase of precipitation
564 would decrease model efficiency because precipitation was interpolated based on elevation, after which the proportion of
565 precipitation falling as snow was redistributed based on the lidar snow depths (see section 3.3). Uncertainties in either data
566 products or in the spatial extrapolation thereof will have decreased the model efficiency. Second, the simulated snow depths
567 reflect all processes occurring in each 10-m grid cell (our model resolution), whereas the ultrasonic snow depth measurements
568 represent processes at ~1-3 m². Small differences between the simulated and observed snow depths are therefore expected.
569 Third, iSnobal is a mass and energy balance model, and therefore optimized to correctly model mass. Model evaluation using
570 snow depths (instead of SWE) is thus less favourable, since small differences in snow densities and SWE could lead to
571 significant differences in snow depths. However, since snow depth measurements were available and SWE measurements
572 were not, we focused on snow depth. Uncertainties were also present in the weather station snow depths, as well as the lidar-
573 based snow depths and the satellite-based SCA analysis. We compared the spatial patterns from the lidar and satellite imagery
574 to test if the spatial pattern was consistent between these two data sources and found this to largely be the case (Fig.-2). As
575

Formatted: Font color: Auto

Formatted: Font color: Auto

576 such, we are confident that despite the uncertainties of our analysis, we captured the within-catchment variability of the
577 snowpack and also adequately modelled the variability in SWI that we set out to investigate.

578
579 Discrepancies between simulated and observed snow depths are challenging to solve, especially for areas with an ephemeral
580 snow cover (Kormos et al., 2014) or with complex vegetation patterns, such as the sagebrush in Johnston Draw. Shallow snow
581 covers are more sensitive to small variations in energy fluxes than deeper seasonal snow covers (Pomeroy et al., 2003; Williams
582 et al., 2009)(Pomeroy et al., 2003; Williams et al., 2009). As a result, small errors in the spatial extrapolation of the forcing
583 data or in the forcing data itself (e.g., uncertainty in the observed relative humidity or temperature) can result in large introduce
584 uncertainties in the model results (Kormos et al., 2014). For instance, the transition from snow-covered to snow-free areas
585 results in a large change in albedo, which influences solar radiative fluxes. The snowpack at the rain-snow transition zone can
586 melt out several times per year, even within a single day, and melt-out dates are variable across the catchment. Therefore, a
587 small error in the simulated melt-out date for each cell can result in a larger error in the basin-average or yearly results. Perhaps
588 these challenges are also a reason for the limited number of studies that have simulated warm snowpacks (Kormos et al., 2014;
589 Kelleners et al., 2010), despite multiple regional studies highlighting that the rain-snow transition zone is expanding and that
590 their climates are changing rapidly (Klos et al., 2014; Nolin and Daly, 2006). Challenges linked to snow ephemerality likely
591 also affected our results, but the agreement between the observed and simulated snow depths indicates that at least the general
592 patterns of accumulation and melt in space and over time were represented by the simulations, at a scale that was small enough
593 to characterize the snow drifts.

594
595 Regardless of the challenges that come with studying an intermittent snow cover, the relationship between the snowpack melt-
596 out date and stream dry-out date poses interesting opportunities to inform hydrological models or evaluate model results with
597 independent observations. Measurements of SCA can be obtained through satellite imagery and are thus easier and cheaper to
598 obtain than SWE or snow depth measurements (e.g., Elder et al., 1991). Satellite observations can be particularly helpful to
599 investigate remote areas that exceed a feasible modelling domain, and can be used to inform or evaluate models. Given the
600 restrictions for satellite imagery imposed by clouds and visit-frequency, particularly for areas with an ephemeral snow cover
601 that might melt out in a single day, a combination of satellite imagery and snowpack modelling seems a promising way to
602 leverage these observations while ensuring the fine temporal resolution that might be needed to study stream cessation.

604 6. Conclusions

605 As a result of climate change, the rain-snow transition zone will receive more rain and less snow, which ~~influence~~ may
606 influence the spatial and temporal distribution of surface water inputs (SWI, summation of rainfall and snowmelt). The goal
607 of this work was to quantify the spatial and temporal distribution of SWI at the rain-snow transition zone, and to assess the
608 sensitivity of annual stream discharge and stream cessation to the temporal distribution of SWI as well as to the annual snowfall
609 fraction. To this end, we used a spatially distributed snowpack model to simulate SWI during five years, of which four had
610 contrasting climatological conditions. We found that the spatial pattern of SWI was similar between years, and that snow
611 drifting and aspect-controlled processes caused large differences in SWI across the watershed. Some areas Snow drifts received
612 up to six times more SWI than other sites, and the difference between SWI from the snow drifts and catchment average SWI
613 was highest for the year with the highest snowfall fraction. This highlights that the snowfall fraction affects temporal and
614 spatial variability in SWI, with more rain leading to less variability. The majority of SWI occurred in winter or spring, which
615 was also the time that the percentage of SWI becoming streamflow was highest (up to 94% in April 2011). Despite similar
616 the 2004-2014 data record, annual SWI (553 vs. 557 mm) and a similar timing of SWI (majority of SWI in spring), snowy
617 2010 had about twice as much stream discharge as rainy 2005. However, in contrast was insensitive to our hypothesis, years
618 with a lower snowfall fraction did not always have lower discharge nor earlier stream drying in summer. This highlights the
619 potential importance of where SWI reaches the ground surface, in addition to when and depended more on total and how much

620 ~~SWI occurs. We found that the spring precipitation. The stream~~ dry-out date ~~at the catchment outlet was was also sensitive to~~
621 ~~total and spring precipitation. In addition, stream cessation was~~ positively correlated to the last day at which there was snow
622 present anywhere in the catchment. ~~These results highlight, which indicates that the persistence of snow drifts in small parts~~
623 ~~of the catchment is critical for sustaining streamflow. This study highlights~~ the heterogeneity of SWI at the rain-snow transition
624 zone and its impact on stream discharge, and thus the need for spatially and temporally representing SWI in headwater-scale
625 studies that simulate streamflow.

626 **Data availability**

627 The hydrometeorological and discharge data used in this paper is available via Godsey et al. (2018), satellite imagery can be
628 obtained via [Planet Team \(2018\)](#) [Planet Team \(2018\)](#) and remaining data is available upon reasonable request.

629 **Author contribution**

630 LK developed the concept of the study together with SEG. LK, SH, ET, AH and KH performed and/or contributed to the
631 simulations. LK prepared the first draft of the manuscript. All co-authors provided recommendations for the data analysis,
632 participated in discussions about the results, and edited the manuscript.

634 **Competing interests**

635 The authors declare that they have no conflict of interest.

636 **Financial support**

637 This research has been supported by the Swiss National Science Foundation (grant no. P2ZHP2_191376) [and the US National](#)
638 [Science Foundation \(award EAR-1653998\)](#).

639 **Bibliography**

640 [Baker, D. B., Richards, R. P., Loftus, T. T., and Kramer, J. W.: A New Flashiness Index: Characteristics and Applications to](#)
641 [Midwestern Rivers and Streams, J Am Water Resources Assoc. 40, 503–522, \[1688.2004.tb01046.x, 2004.\]\(https://doi.org/10.1111/j.1752-
642 <a href=\)](#)

643 Barnett, T. P., Adam, J. C., and Lettenmaier, D. P.: Potential impacts of a warming climate on water availability in snow-
644 dominated regions, *Nature*, 438, 303–309, <https://doi.org/10.1038/nature04141>, 2005.

645 Bavay, M., Grünewald, T., and Lehning, M.: Response of snow cover and runoff to climate change in high Alpine
646 catchments of Eastern Switzerland, *Adv. Water Resour.*, 55, 4–16, <https://doi.org/10.1016/j.advwatres.2012.12.009>, 2013.

647 Beniston, M., Keller, F., Koffi, B., and Goyette, S.: Estimates of snow accumulation and volume in the Swiss Alps under
648 changing climatic conditions, *Theor. Appl. Climatol.*, 76, 125–140, <https://doi.org/10.1007/s00704-003-0016-5>, 2003.

649 Berghuijs, W. R., Woods, R. A., and Hrachowitz, M.: A precipitation shift from snow towards rain leads to a decrease in
650 streamflow, *Nature Clim. Change*, 4, 583–586, <https://doi.org/10.1038/nclimate2246>, 2014.

Formatted: Font color: Auto, Not Highlight

651 Bilish, S. P., Callow, J. N., and McGowan, H. A.: Streamflow variability and the role of snowmelt in a marginal snow
652 environment, *Arct. Antarct. Alp. Res.*, 52, 161–176, <https://doi.org/10.1080/15230430.2020.1746517>, 2020.

653 Chauvin, G. M., Flerchinger, G. N., Link, T. E., Marks, D., Winstral, A. H., and Seyfried, M. S.: Long-term water balance
654 and conceptual model of a semi-arid mountainous catchment, *J. Hydrol.*, 400, 133–143,
655 <https://doi.org/10.1016/j.jhydrol.2011.01.031>, 2011.

656 Christensen, N. S., Wood, A. W., Voisin, N., Lettenmaier, D. P., and Palmer, R. N.: The Effects of Climate Change on the
657 Hydrology and Water Resources of the Colorado River Basin, *ClimaticClimat. Change*, 62, 337–363,
658 <https://doi.org/10.1023/B:CLIM.0000013684.13621.1f>, 2004.

659 Datry, T., Larned, S. T., and Tockner, K.: Intermittent Rivers: A Challenge for Freshwater Ecology, *BioScience*, 64, 229–
660 235, <https://doi.org/10.1093/biosci/bit027>, 2014.

661 Deems, J. S., Painter, T. H., and Finnegan, D. C.: Lidar measurement of snow depth: a review, *J. Glaciol.*, 59, 467–479,
662 <https://doi.org/10.3189/2013JG12J154>, 2013.

663 Elder, K., Dozier, J., and Michaelsen, J.: Snow accumulation and distribution in an Alpine Watershed, *Water Resour. Res.*,
664 27, 1541–1552, <https://doi.org/10.1029/91WR00506>, 1991.

665 Esri Inc.: ArcMap (version 10.7.1), 2020.

666 Fang, X. and Pomeroy, J. W.: Modelling blowing snow redistribution to prairie wetlands, *Hydrol. Process.*, 23, 2557–2569,
667 <https://doi.org/10.1002/hyp.7348>, 2009.

668 Flerchinger, G. N. and Cooley, K. R.: A ten-year water balance of a mountainous semi-arid watershed, *J. Hydrol.*, 237, 86–
669 99, [https://doi.org/10.1016/S0022-1694\(00\)00299-7](https://doi.org/10.1016/S0022-1694(00)00299-7), 2000.

670 Flerchinger, G. N., Cooley, K. R., and Ralston, D. R.: Groundwater response to snowmelt in a mountainous watershed, *J.*
671 *Hydrol.*, 133, 293–311, [https://doi.org/10.1016/0022-1694\(93\)90146-Z](https://doi.org/10.1016/0022-1694(93)90146-Z), 1992.

672 Godsey, S. E., Marks, D., Kormos, P. R., Seyfried, M. S., Enslin, C. L., Winstral, A. H., McNamara, J. P., and Link, T. E.:
673 Eleven years of mountain weather, snow, soil moisture and streamflow data from the rain–snow transition zone – the
674 Johnston Draw catchment, Reynolds Creek Experimental Watershed and Critical Zone Observatory, USA, *Earth Syst. Sci.*
675 *Data*, 10, 2018.

676 Grünewald, T., Bühler, Y., and Lehning, M.: Elevation dependency of mountain snow depth, *Cryosphere*, 8, 2381–2394,
677 <https://doi.org/10.5194/tc-8-2381-2014>, 2014.

678 Hammond, J. C., Harpold, A. A., Weiss, S., and Kampf, S. K.: Partitioning snowmelt and rainfall in the critical zone: effects
679 of climate type and soil properties, *Hydrol. Earth Syst. Sci.*, 23, 3553–3570, <https://doi.org/10.5194/hess-23-3553-2019>,
680 2019.

681 Hartman, M. D., Baron, J. S., Lammers, R. B., Cline, D. W., Band, L. E., Liston, G. E., and Tague, C.: Simulations of snow
682 distribution and hydrology in a mountain basin, *Water Resour. Res.*, 35, 1587–1603,
683 <https://doi.org/10.1029/1998WR900096>, 1999.

684 Havens, S., Marks, D., Kormos, P., and Hedrick, A.: Spatial Modeling for Resources Framework (SMRF): A modular
685 framework for developing spatial forcing data for snow modeling in mountain basins, *Comput. and Geosci.*, 109, 295–304,
686 <https://doi.org/10.1016/j.cageo.2017.08.016>, 2017.

687 Havens, S., Marks, D., Sandusky, M., Hedrick, A., Johnson, M., Robertson, M., and Trujillo, E.: Automated Water Supply
688 Model (AWSM): Streamlining and standardizing application of a physically based snow model for water resources and
689 reproducible science, *Comput. and Geosci.*, 144, 104571, <https://doi.org/10.1016/j.cageo.2020.104571>, 2020.

690 Hedrick, A. R., Marks, D., Marshall, H., McNamara, J., Havens, S., Trujillo, E., Sandusky, M., Robertson, M., Johnson, M.,
691 Bormann, K. J., and Painter, T. H.: From Drought to Flood: A Water Balance Analysis of the Tuolumne River Basin during
692 Extreme Conditions (2015 – 2017), *Hydrological Processes*, hyp.13749, <https://doi.org/10.1002/hyp.13749>, 2020.

693 Jasechko, S., Birks, S. J., Gleeson, T., Wada, Y., Fawcett, P. J., Sharp, Z. D., McDonnell, J. J., and Welker, J. M.: The
694 pronounced seasonality of global groundwater recharge, *Water Resour. Res.*, 50, 8845–8867,
695 <https://doi.org/10.1002/2014WR015809>, 2014.

696 Johnson, G. L. and Hanson, C. L.: Topographic and atmospheric influences on precipitation variability over a mountainous
697 watershed, *J. Appl. Meteor.*, 34, 68–86, 1995.

698 Kelleners, T. J., Chandler, D. G., McNamara, J. P., Gribb, M. M., and Seyfried, M. S.: Modeling Runoff Generation in a
699 Small Snow-Dominated Mountainous Catchment, *Vadose Zone J.*, 9, 517–527, <https://doi.org/10.2136/vzj2009.0033>, 2010.

700 Klos, P. Z., Link, T. E., and Abatzoglou, J. T.: Extent of the rain-snow transition zone in the western U.S. under historic and
701 projected climate: Climatic rain-snow transition zone, *Geophys. Res. Lett.*, 41, 4560–4568,
702 <https://doi.org/10.1002/2014GL060500>, 2014.

703 Kormos, P. R., Marks, D., McNamara, J. P., Marshall, H. P., Winstral, A., and Flores, A. N.: Snow distribution, melt and
704 surface water inputs to the soil in the mountain rain–snow transition zone, *J. Hydrol.*, 519, 190–204,
705 <https://doi.org/10.1016/j.jhydrol.2014.06.051>, 2014.

706 Kormos, P. R., Luce, C. H., Wenger, S. J., and Berghuijs, W. R.: Trends and sensitivities of low streamflow extremes to
707 discharge timing and magnitude in Pacific Northwest mountain streams, *Water Resour. Res.*, 52, 4990–5007,
708 <https://doi.org/10.1002/2015WR018125>, 2016.

709 Kretchun, A. M., Scheller, R. M., Shinneman, D. J., Soderquist, B., Maguire, K., Link, T. E., and Strand, E. K.: Long term
710 persistence of aspen in snowdrift-dependent ecosystems, *Forest Ecology and Management*, *For. Ecol. Manag.*, 462,
711 118005, <https://doi.org/10.1016/j.foreco.2020.118005>, 2020.

712 Leung, L. R., Qian, Y., Bian, X., Washington, W. M., Han, J., and Roads, J. O.: Mid-Century Ensemble Regional Climate
713 Change Scenarios for the Western United States, *Climatic Clim. Change*, 62, 75–113,
714 <https://doi.org/10.1023/B:CLIM.0000013692.50640.55>, 2004.

715 López-Moreno, J. I. and Stähli, M.: Statistical analysis of the snow cover variability in a subalpine watershed: Assessing the
716 role of topography and forest interactions, *J. Hydrol.*, 348, 379–394, <https://doi.org/10.1016/j.jhydrol.2007.10.018>, 2008.

717 Luce, C. H. and Holden, Z. A.: Declining annual streamflow distributions in the Pacific Northwest United States, 1948–
718 2006, *Geophys. Res. Lett.*, 36, L16401, <https://doi.org/10.1029/2009GL039407>, 2009.

719 MacNeille, R. B., Lohse, K. A., Godsey, S. E., Perdrial, J. N., and Baxter, C. N.: Influence of drying and wildfire on
720 longitudinal chemistry patterns and processes of intermittent streams, *Frontiers in Front. Water*,
721 <https://doi.org/10.3389/frwa.2020.563841>, 2020.

722 Marks, D., Domingo, J., Susong, D., Link, T., and Garen, D.: A spatially distributed energy balance snowmelt model for
723 application in mountain basins, *Hydrol. Process.*, 13, 26, 1999.

724 Marks, D., Winstral, A., and Seyfried, M.: Simulation of terrain and forest shelter effects on patterns of snow deposition,
725 snowmelt and runoff over a semi-arid mountain catchment, *Hydrol. Process.*, 16, 3605–3626,
726 <https://doi.org/10.1002/hyp.1237>, 2002.

727 Marks, D., Winstral, A., Reba, M., Pomeroy, J., and Kumar, M.: An evaluation of methods for determining during-storm
728 precipitation phase and the rain/snow transition elevation at the surface in a mountain basin, *Advances in Adv. Water*
729 *Resources-Resour.*, 55, 98–110, <https://doi.org/10.1016/j.advwatres.2012.11.012>, 2013.

730 Marshall, A. M., Link, T. E., Abatzoglou, J. T., Flerchinger, G. N., Marks, D. G., and Tedrow, L.: Warming Alters
731 Hydrologic Heterogeneity: Simulated Climate Sensitivity of Hydrology-Based Microrefugia in the Snow-to-Rain Transition
732 Zone, *Water Resour. Res.*, 55, 2122–2141, <https://doi.org/10.1029/2018WR023063>, 2019.

733 McCabe, G. J. and Clark, M. P.: Trends and Variability in Snowmelt Runoff in the Western United States, *J. Hydromet.*, 6,
734 476–482, <https://doi.org/10.1175/JHM428.1>, 2005.

735 McCabe, G. J., Wolock, D. M., Pederson, G. T., Woodhouse, C. A., and McAfee, S.: Evidence that Recent Warming is
736 Reducing Upper Colorado River Flows, *Earth Interact.*, 21, 1–14, <https://doi.org/10.1175/EI-D-17-0007.1>, 2017.

737 McNamara, J. P., Chandler, D., Seyfried, M., and Achet, S.: Soil moisture states, lateral flow, and streamflow generation in a
738 semi-arid, snowmelt-driven catchment, *Hydrol. Process.*, 19, 4023–4038, <https://doi.org/10.1002/hyp.5869>, 2005.

739 Milly, P. C. D. and Dunne, K. A.: Colorado River flow dwindles as warming-driven loss of reflective snow energizes
740 evaporation, *Science*, 367, 1252–1255, <https://doi.org/10.1126/science.aay9187>, 2020.

741 Molotch, N. P., Brooks, P. D., Burns, S. P., Litvak, M., Monson, R. K., McConnell, J. R., and Musselman, K.:
742 Ecohydrological controls on snowmelt partitioning in mixed-conifer sub-alpine forests, *Ecohydrol.*, 2, 129–142,
743 <https://doi.org/10.1002/eco.48>, 2009.

744 Mott, R., Vionnet, V., and Grünwald, T.: The Seasonal Snow Cover Dynamics: Review on Wind-Driven Coupling
745 Processes, *Front. Earth Sci.*, 6, 197, <https://doi.org/10.3389/feart.2018.00197>, 2018.

746 Nash, J. E. and Sutcliffe, J. V.: River flow forecasting through conceptual models part I -A discussion of principles, *J.*
747 *Hydrol.*, 10, 282–290, 1970.

748 Nayak, A., Marks, D., Chandler, D. G., and Seyfried, M.: Long-term snow, climate, and streamflow trends at the Reynolds
749 Creek Experimental Watershed, Owyhee Mountains, Idaho, United States, *Water Resour. Res.*, 46,
750 <https://doi.org/10.1029/2008WR007525>, 2010.

751 Naz, B. S., Kao, S.-C., Ashfaq, M., Rastogi, D., Mei, R., and Bowling, L. C.: Regional hydrologic response to climate
752 change in the conterminous United States using high-resolution hydroclimate simulations, *Global and Planetary Glob.*
753 *Planet. Change*, 143, 100–117, <https://doi.org/10.1016/j.gloplacha.2016.06.003>, 2016.

754 Nolin, A. W. and Daly, C.: Mapping “At Risk” Snow in the Pacific Northwest, *J. Hydromet.*, 7, 1164–1171,
755 <https://doi.org/10.1175/JHM543.1>, 2006.

756 Parr, C., Sturm, M., and Larsen, C.: Snowdrift Landscape Patterns: An Arctic Investigation, *Water Resour. Res.*, 56,
757 <https://doi.org/10.1029/2020WR027823>, 2020.

758 Patton, N. R., Lohse, K. A., Seyfried, M. S., Godsey, S. E., and Parsons, S. B.: Topographic controls of soil organic carbon
759 on soil-mantled landscapes, *Sci Rep*, 9, 6390, <https://doi.org/10.1038/s41598-019-42556-5>, 2019.

760 Pflug, J. M. and Lundquist, J. D.: Inferring Distributed Snow Depth by Leveraging Snow Pattern Repeatability: Investigation
761 Using 47 Lidar Observations in the Tuolumne Watershed, Sierra Nevada, California, *Water Resour. Res.*, 56,
762 e2020WR027243, <https://doi.org/10.1029/2020WR027243>, 2020.

763 Pierson, F. B. and Cram, Z. K.: Reynolds Creek Experimental Watershed Runoff and Sediment Data Collection Field
764 Manual, Northwest Watershed research Center, USDA-ARS, Boise, Idaho, 1998.

765 Pierson, F. B., Slaughter, C. W., and Cram, Z. K.: Monitoring Discharge and Suspended Sediment, Reynolds Creek
766 Experimental Watershed, Idaho, USA, Northwest Watershed Research Center USDA-Agricultural Research Service, Boise,
767 Idaho, 2000.

768 Planet Application Program Interface: In Space for Life on Earth. San Francisco, CA.: <https://api.planet.com>.

769 Pomeroy, J. W., Toth, B., Granger, R. J., Hedstrom, N. R., and Essery, R. L. H.: Variation in Surface Energetics during
770 Snowmelt in a Subarctic Mountain Catchment, *J. Hydromet.*, 4, 18, 2003.

771 Regonda, S. K., Rajagopalan, B., Clark, M., and Pitlick, J.: Seasonal Cycle Shifts in Hydroclimatology over the Western
772 United States, *J. Clim.*, 18, 372–384, <https://doi.org/10.1175/JCLI-3272.1>, 2005.

773 Schirmer, M., Wirz, V., Clifton, A., and Lehning, M.: Persistence in intra-annual snow depth distribution: 1.
774 Measurements and topographic control, *Water Resour. Res.*, 47, <https://doi.org/10.1029/2010WR009426>, 2011.

775 Schweizer, J., Jamieson, J. B., and Schneebeli, M.: Snow avalanche formation, *Rev. Geophys.*, 41, 1016,
776 <https://doi.org/10.1029/2002RG000123>, 2003.

777 Seager, R., Naik, N., and Vogel, L.: Does Global Warming Cause Intensified Interannual Hydroclimate Variability?, *J. of*
778 *Climate*, 25, 3355–3372, <https://doi.org/10.1175/JCLI-D-11-00363.1>, 2012.

779 Seyfried, M., Chandler, D., and Marks, D.: Long-Term Soil Water Trends across a 1000-m Elevation Gradient, *Vadose Zone*
780 *Journal*, 10, 1276–1286, <https://doi.org/10.2136/vzj2011.0014>, 2011.

781 ~~Seyfried, M., Flerchinger, G., Bryden, S., Link, T., Marks, D., and McNamara, J.: Slope/Aspect Controls on Soil Climate:
782 Field Documentation and Implications for Large-Scale Simulation of Critical Zone Processes. *Vadose Zone J.*,
783 <https://doi.org/10.1002/vzj2.20158>, 2021.~~

784 Seyfried, M. S., Grant, L. E., Marks, D., Winstral, A., and McNamara, J.: Simulated soil water storage effects on streamflow
785 generation in a mountainous snowmelt environment, Idaho, USA, *Hydrol. Process.*, 23, 858–873,
786 <https://doi.org/10.1002/hyp.7211>, 2009.

787 ~~Seyfried, M. S., Flerchinger, G. N., Bryden, S., Link, T. E., Marks, D. G., and McNamara, J. P.: Slope/Aspect
788 Controls on Soil Climate: Field Documentation and Implications for Large Scale Simulation of Critical Zone
789 Processes, in review.~~

790 Shrestha, R. and Glenn, N. F.: 2007 Lidar-Derived Digital Elevation Model, Canopy Height Model and Vegetation Cover
791 Model Data Sets for Reynolds Creek Experimental Watershed, Southwestern Idaho [Data set],
792 <https://doi.org/10.18122/B27C77>, 2016.

793 Somers, L. D. and McKenzie, J. M.: A review of groundwater in high mountain environments, *WIREs Water*, 7,
794 <https://doi.org/10.1002/wat2.1475>, 2020.

795 Stephenson, G. R.: Soil-Geology_vegetation Inventories for Reynolds Creek Watershed, Agric. Exp. Stn. Univ. Idaho Coll.
796 Agric., 1970.

797 Stewart, I. T.: Changes in snowpack and snowmelt runoff for key mountain regions, [Hydrological Processes,Hydrolog.
798 Process.](https://doi.org/10.1002/hyp.7128), 23, 78–94, <https://doi.org/10.1002/hyp.7128>, 2009.

799 Stewart, I. T., Cayan, D. R., and Dettinger, M. D.: Changes toward Earlier Streamflow Timing across Western North
800 America, *J. Clim.*, 18, 1136–1155, <https://doi.org/10.1175/JCLI3321.1>, 2005.

801 Sturm, M.: White water: Fifty years of snow research in WRR and the outlook for the future, *Water Resour. Res.*, 51, 4948–
802 4965, <https://doi.org/10.1002/2015WR017242>, 2015.

803 Sturm, M. and Wagener, A. M.: Using repeated patterns in snow distribution modeling: An Arctic example, 46, W12549,
804 <https://doi.org/10.1029/2010WR009434>, 2010.

805 Tennant, C. J., Harpold, A. A., Lohse, K. A., Godsey, S. E., Crosby, B. T., Larsen, L. G., Brooks, P. D., Van Kirk, R. W.,
806 and Glenn, N. F.: Regional sensitivities of seasonal snowpack to elevation, aspect, and vegetation cover in western North
807 America, *Water Resour. Res.*, 53, 6908–6926, <https://doi.org/10.1002/2016WR019374>, 2017.

808 Trujillo, E., Ramírez, J. A., and Elder, K. J.: Topographic, meteorologic, and canopy controls on the scaling characteristics
809 of the spatial distribution of snow depth fields: ~~SPATIAL SCALING OF SNOW DEPTH~~[spatial scaling of snow depth](https://doi.org/10.1029/2006WR005317),
810 *Water Resour. Res.*, 43, <https://doi.org/10.1029/2006WR005317>, 2007.

811 Trujillo, E., Havens, S., Hedrick, A. R., Johnson, M., Robertson, M., Pierson, F. B., and Marks, D. G.: Utilizing spatially
812 resolved SWE to inform snowfall interpolation across a headwater catchment in the Sierra Nevada - [AGU Fall meeting](https://doi.org/10.1029/2019AGUFM.C33B1579T),
813 C33B-1579, <https://doi.org/10.1029/2019AGUFM.C33B1579T>, 2019.

814 Viviroli, D., Dürr, H. H., Messerli, B., Meybeck, M., and Weingartner, R.: Mountains of the world, water towers for
815 humanity: Typology, mapping, and global significance, *Water Resources Research, Resour. Res.*, 43,
816 <https://doi.org/10.1029/2006WR005653>, 2007.

817 Vögeli, C., Lehning, M., Wever, N., and Bavay, M.: Scaling Precipitation Input to Spatially Distributed Hydrological
818 Models by Measured Snow Distribution, *Front. Earth Sci.*, 4, <https://doi.org/10.3389/feart.2016.00108>, 2016.

819 ~~Wang, R., Kumar, M., and Marks, D.: Anomalous trend in soil evaporation in a semi-arid, snow-dominated
820 watershed, *Advances in Water Resources*, 57, 32–40, <https://doi.org/10.1016/j.advwatres.2013.03.004>, 2013.~~

821 Westerling, A. L., Hidalgo, H. G., Cayan, D. R., and Swetnam, T. W.: Warming and Earlier Spring Increase Western U.S.
822 Forest Wildfire Activity, *Science*, 313, 940–943, <https://doi.org/10.1126/science.1128834>, 2006.

823 Williams, C. J., McNamara, J. P., and Chandler, D. G.: Controls on the temporal and spatial variability of soil moisture in a
824 mountainous landscape: the signature of snow and complex terrain, *Hydrology and Earth System Sciences*, 13, 1325–1336,
825 <https://doi.org/10.5194/hess-13-1325-2009>, 2009.

826 Winstral, A. and Marks, D.: Simulating wind fields and snow redistribution using terrain-based parameters to model snow
827 accumulation and melt over a semi-arid mountain catchment, *Hydrol. Process.*, 16, 3585–3603,
828 <https://doi.org/10.1002/hyp.1238>, 2002.

829 Winstral, A. and Marks, D.: Long-term snow distribution observations in a mountain catchment: Assessing variability, time
830 stability, and the representativeness of an index site, *Water Resour. Res.*, 50, 293–305,
831 <https://doi.org/10.1002/2012WR013038>, 2014.

832
833
834

Formatted: Font color: Auto, Not Highlight

835 Tables

836 **Table 1. Precipitation, discharge and SWI characteristics for each water year including: total precipitation (mm), the**
 837 **fraction of precipitation falling as snow (snowfall fraction), dates of the start (snow_{start}) and end (snow_{end}) of the snowy**
 838 **season, defined as > 1 cm of snow at weather station jdt124b (except for 2005, for which only data for weather station**
 839 **jdt125 was available), dates at which the simulated snow cover had melted (melt-out date; SCA = 0), annual discharge**
 840 **(Q_{annual}) and runoff efficiency (Q_{annual}/SWI_{avg}) as well as the start (Flow_{start}) and end (Flow_{end}) of surface flow at the**
 841 **catchment outlet, and simulated surface water inputs (SWI). We report the catchment-average SWI (SWI_{avg}) as well**
 842 **as SWI from rain (SWI_{rain}), SWI from snowmelt (SWI_{snow}), the 98th percentile of SWI (SWI₉₈), maximum SWI**
 843 **(SWI_{max}) and the average SWI for north-facing slopes (excluding the drift area, SWI_{NF-drift}) and south-facing slopes**
 844 **(SWI_{SF}).**
 845

WY		2005	2009	2010	2011	2014
		Rainy	Lidar available	Snowy	Wet	Dry
Precipitation	mm	542	549	531	693	450
Snowfall fraction	-	0.23	0.49	0.57	0.41	0.30
Snow_{start}	dd-mon	16-Oct* (16)	01-Nov (32)	04-Oct (4)	06-Nov (37)	20-Oct (20)
Snow_{end}	(DOWY)	01-Mar* (152)	19-Apr (201)	26-May (238)	01-May (213)	06-Apr (188)
SCA = 0		02-Jun (245)	14-Jun (257)	16-Jun (259)	18-Jun (261)	14-May (226)
Q_{annual}	mm	62	81	117	307	80
Q/SWI_{avg}	-	0.11	0.14	0.21	0.46	0.16
Flow_{start}	dd-mon	11-Nov (38)	22-Nov (54)	12-Nov (43)	24-Oct (24)	28-Oct (28)
Flow_{end}	(DOWY)	25-Aug (328)	25-Aug (328)	26-Aug (329)	-	13-Jul (285)
SWI_{avg}	mm	557	587	553	672	506
SWI_{snow}	mm	145	271	310	229	170
SWI_{rain}	mm	412	316	243	443	336
SWI₉₈	mm	982	1394	1513	1588	1015
SWI_{max}	mm	2005	3350	3863	3892	2219
SWI_{NF-drift}	mm	551	568	534	665	490
SWI_{SF}	mm	505	456	407	556	430

*dates based on measurements at jdt125 (outlet) rather than 124b (close to top of the catchment, see Fig. 1)

Formatted: Font color: Auto

Formatted Table

Formatted: Font color: Auto

Formatted: Font color: Auto

Formatted: Font color: Auto

846
847
848
849

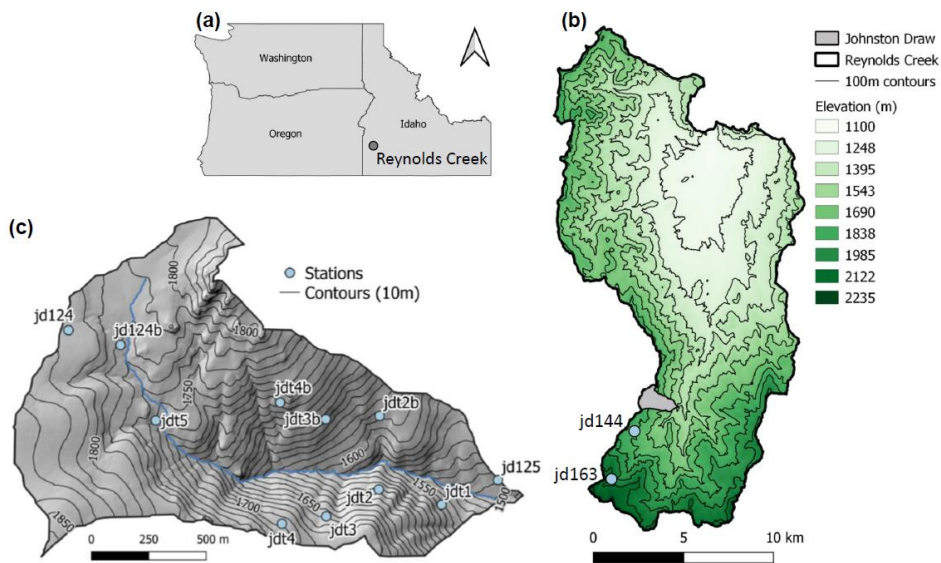
850 Table 2. Nash-Sutcliffe Efficiency's Efficiency (NSE; Nash and Sutcliffe, 1970) and root mean
 851 square error (RMSE, emm) for simulated and observed snow depths at each weather station, as well as the NSE
 852 for the normalized (z-transformed) snow depths (NSE_{norm}). Dashes (-) indicate that no observed snow depths were
 853 available in that year. See Supplement S4 Supplemental Fig. S7 for the time series of observed and simulated snow
 854 depths.
 855

Formatted: Font color: Auto

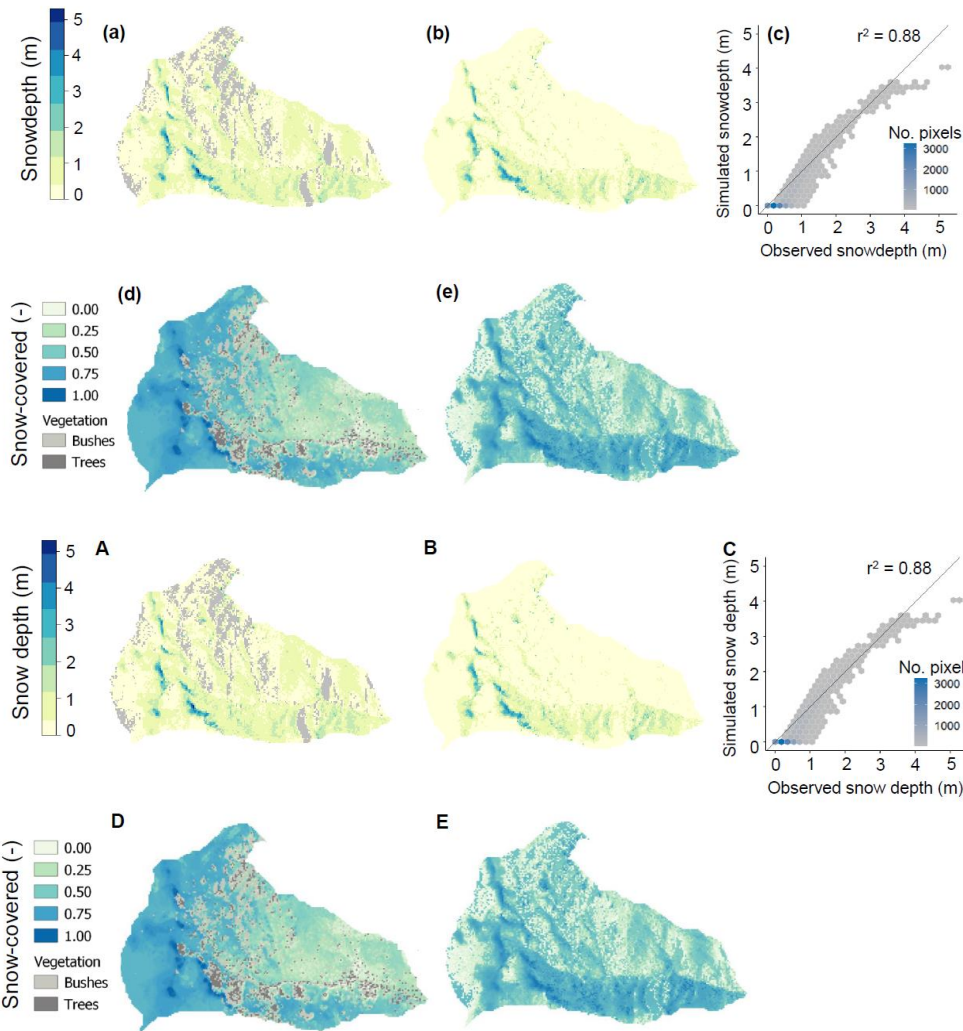
	Station	Outlet		North-facing			South-facing			Upper region		Median
		jd125	jd1	jd2	jd3	jd4	jd2b	jd3b	jd4b	jd5	jd124b	
NSE	2005	0.83	-	-	-	-	-	-	-	-	-	0.83
	2009	0.45	0.67	0.09	0.95	0.91	-	-	-	0.65	0.84	0.67
	2010	0.01	0.92	0.91	0.68	0.86	-	-	-	0.67	0.92	0.86
	2011	0.40	-0.46	0.63	0.03	-9.60	0.52	0.76	0.54	-0.06	-5.56	0.22
	2014	0.80	-2.07	0.76	0.49	0.25	0.39	0.60	0.80	0.81	0.66	0.63
NSE _{norm}	2005	0.87	-	-	-	-	-	-	-	-	-	0.87
	2009	0.65	0.50	0.50	0.83	0.85	-	-	-	0.89	0.97	0.83
	2010	0.25	0.94	0.92	0.96	0.95	-	-	-	0.68	0.94	0.94
	2011	0.86	0.34	0.73	0.89	-0.86	0.55	0.75	0.67	0.63	0.15	0.65
	2014	0.77	0.59	0.75	0.81	0.64	0.33	0.64	0.72	0.80	0.79	0.74
RMSE (emm)	2005	0.801	-	-	-	-	-	-	-	-	-	0.801
	2009	0.115	9.70.1 0	0.194	5.11 0.05	7.90.08	-	-	-	0.114	9.10.0 9	9.70.10
	2010	11.70.1 2	3.70.0 3	5.10.0 5	0.11 4	9.30.09	-	-	-	8.70.0 9	5.60.0 6	8.70.08
	2011	2.90.03 5	0.065 5	4.20.0 4	8.30 .08	0.30.3	2.10. 02	2.10.0 2	1.90.0 2	5.0.05	0.15.0	4.60.08
	2014	1.20.01 6	5.70.0 6	2.0.02	3.60 .04	4.70.05	1.90. 02	2.20.0 2	1.10.0 1	1.60.0 2	2.40.0 2	2.10.03

Formatted Table

856
857

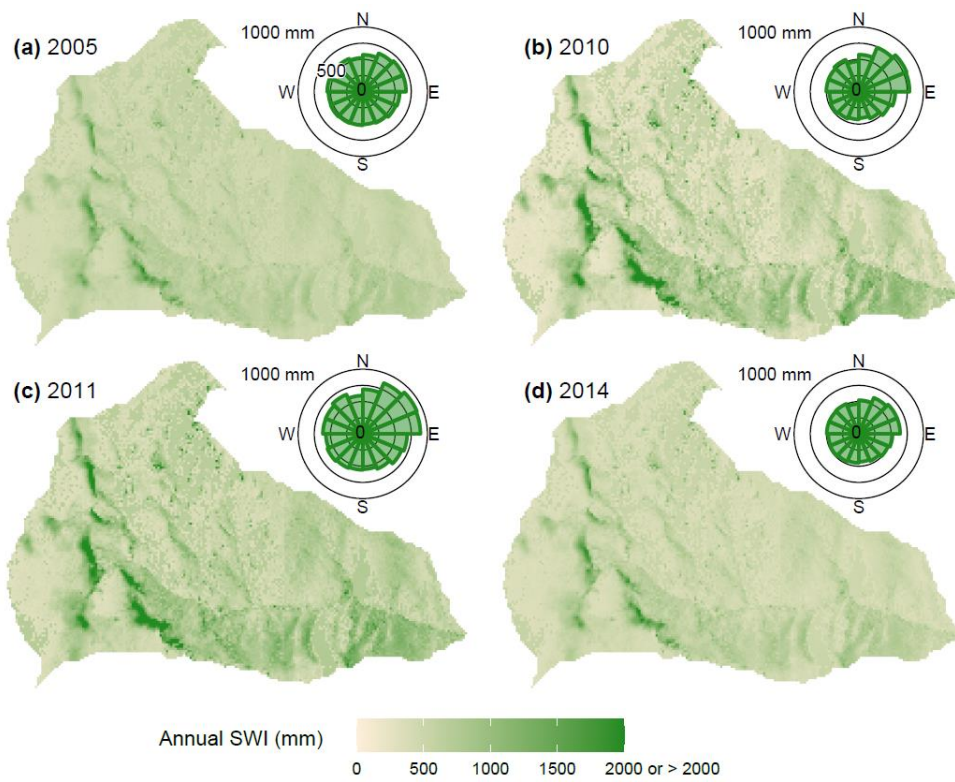


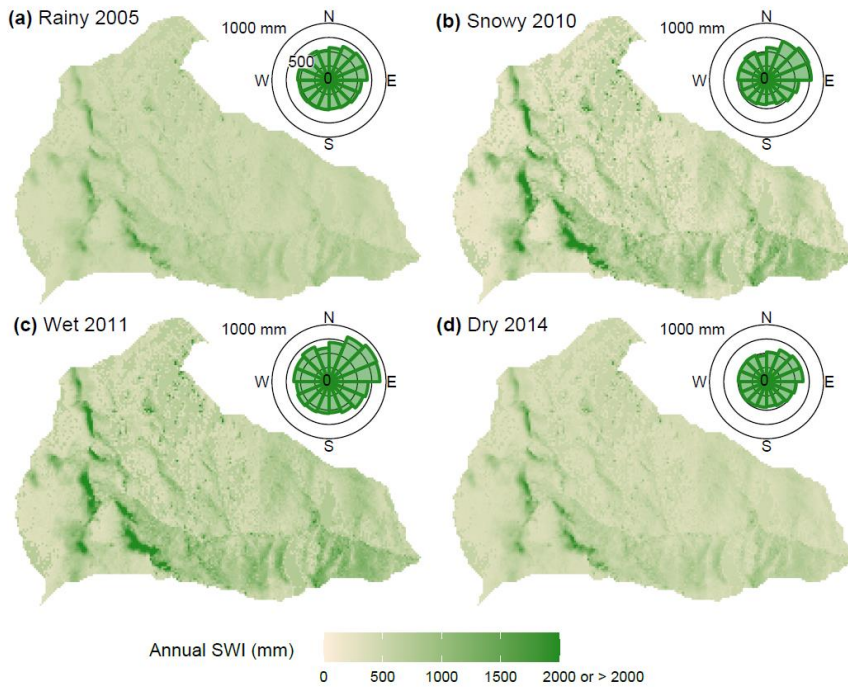
859 **Fig. 1** Maps of the location of (a) the Reynolds Creek Experimental Watershed (RCEW) in the state of Idaho (USA,
 860 **EPSG:4269 - NAD83 projection**), (b) Reynolds Creek Experimental Watershed with indication of elevation (white =
 861 lower, dark green = higher), 100 m contour lines, the location of Johnston Draw (grey polygon) and two additional
 862 precipitation gauges (dots) indicated in light blue, and (c) Johnston Draw with the weather stations (light blue dots),
 863 stream (blue line), and 10 m contour lines (black lines), overlain on a hillshade DEM.
 864
 865



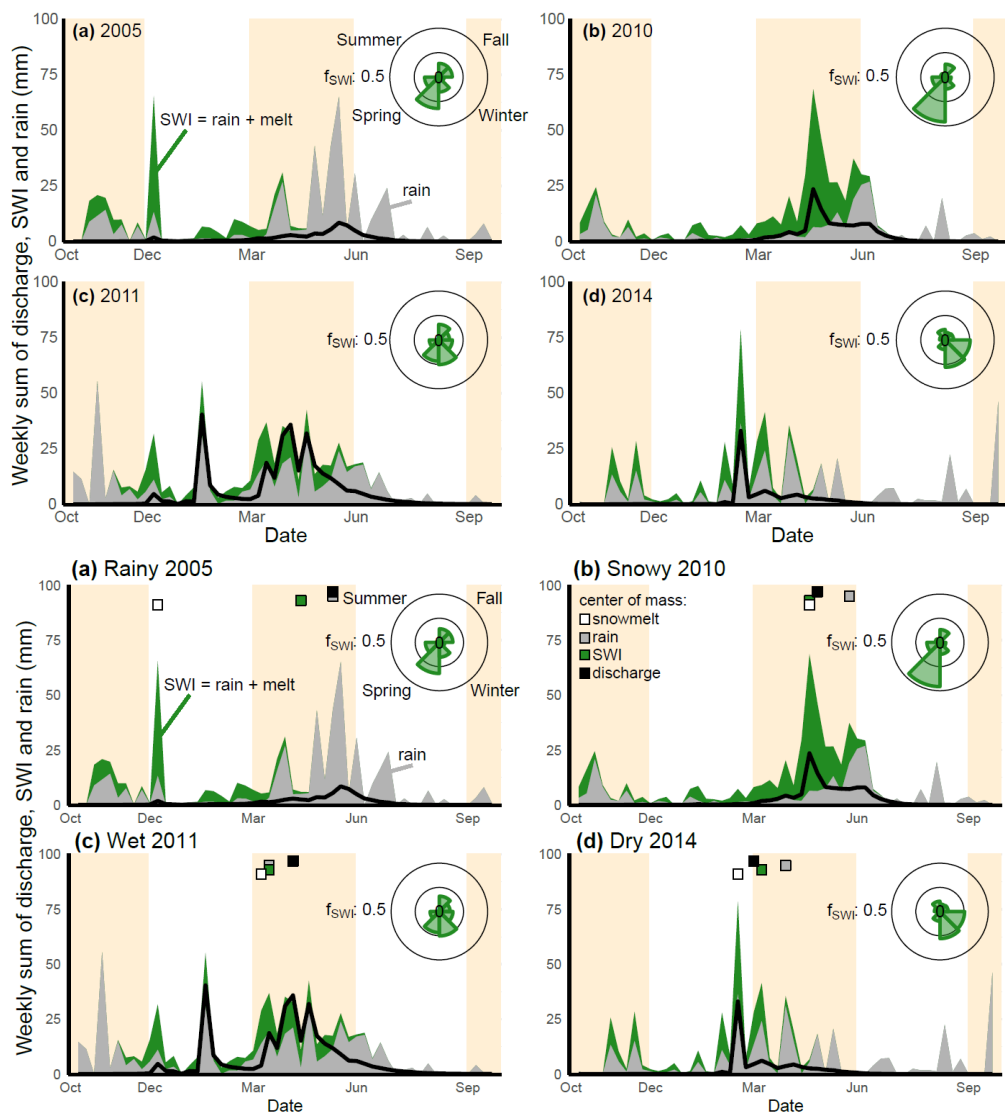
866
867
868 **Fig. 2.** (a) Lidar snow depth (m) at 3-m resolution on 18 March 2009, and (b) simulated snow ~~depth~~**depths** for the same day, where yellow indicates low snow depths, blue high snow depths, and grey the areas for which the snow depth could
869 not reliably be determined from the lidar measurement (see section 3.2). (c) ~~shows a hexagonal~~**Hexagonal** bin plot
870

871 comparing the observed and simulated snow depths with grey colors indicating fewer pixels and blue indicating more
872 pixels included per bin. (d) ~~shows the fraction~~Fraction of images for which sites were snow-covered, using 3-m
873 resolution satellite imagery for the available images (n=41) of water year 2019 (see section 3.2), and (e) ~~shows the~~
874 fraction of time during which each pixel was snow-covered, using the simulated snow cover from the beginning of the
875 water year 2009 until all snow had melted (n=238). Bushes and trees (marked in grey in ~~D~~panel d) inhibited the exact
876 determination of the snow cover for the satellite imagery in some locations.



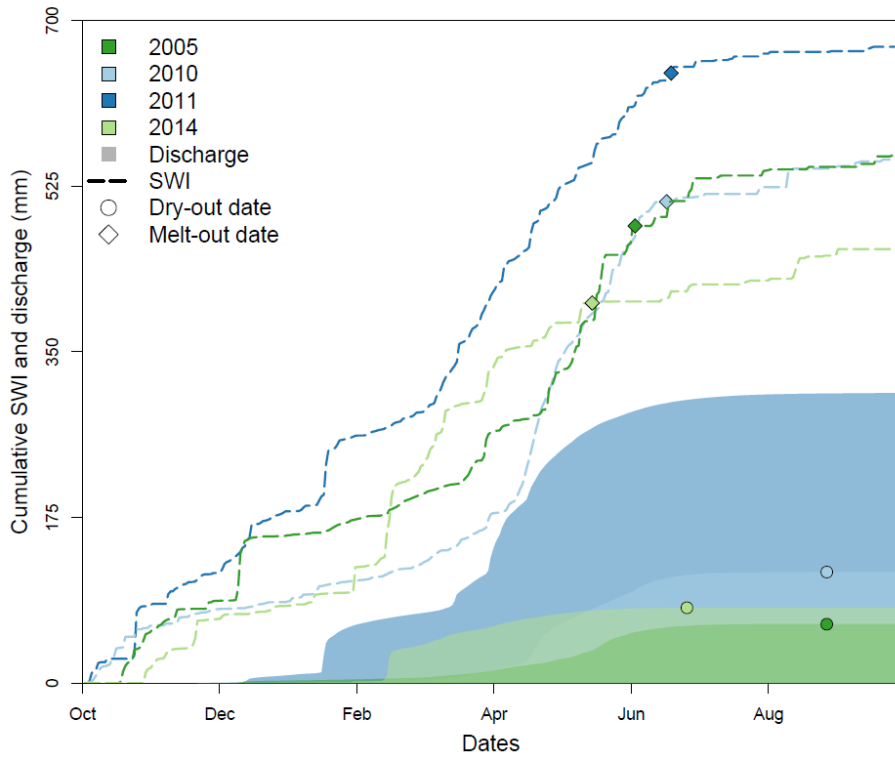


878
 879 **Fig. 3.** Maps showing the yearly sum of surface water inputs (SWI, mm) for (a) rainy 2005, (b) snowy 2010, (c) wet 2011
 880 and (d) dry 2014, with polar diagram insets showing the average sum of SWI per 10-m grid cell for each aspect (binned
 881 per 22.5°). Higher SWI values are shown in darker colours, lower SWI values in lighter colours, and SWI values are
 882 capped at 2000 mm to enhance the contrast. Maximum annual SWI values are shown in Table 1 and a map of simulated
 883 SWI for 2009 is shown in [Supplement-S5Supplemental Fig. S13](#).
 884

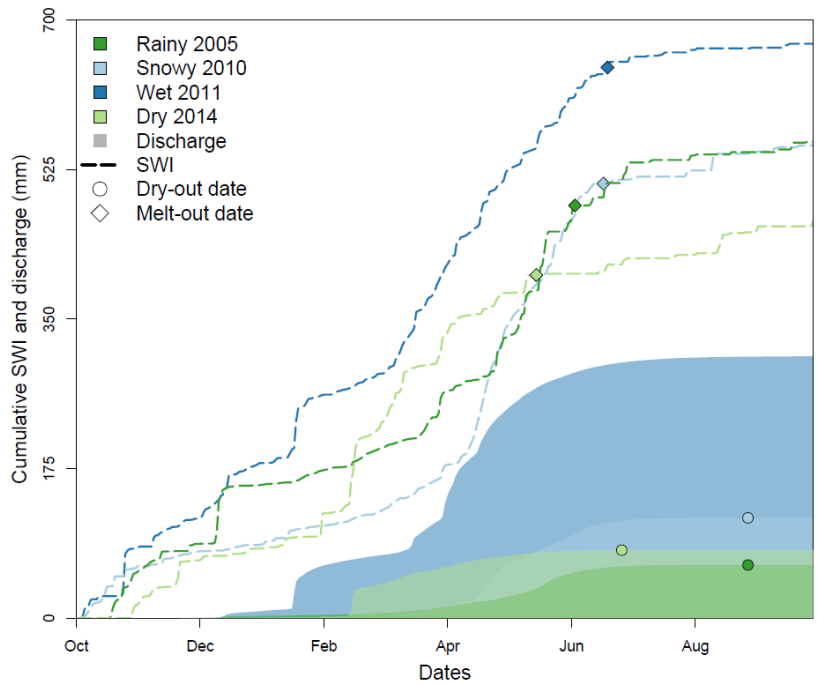


887 Fig. 4 Weekly sums of surface water inputs (SWI, summation of rainfall and snowmelt, green polygons, mm), rainfall
888 (grey polygons, mm) and specific discharge (black line graph, mm) for (a) rainy 2005, (b) snowy 2010, (c) wet 2011 and
889 (d) dry 2014. Background panels are coloured according to the different seasons (fall, winter, spring, summer, fall).
890 The polar diagram insets indicate ~~which~~the fraction of SWI (f_{swi}) ~~occurred in~~ whicheach season. Squares at the top of
891 each panel indicate the annual center of mass for snowmelt (white), rainfall (grey), SWI (green) and discharge (black).
892

893
894



895



896

897

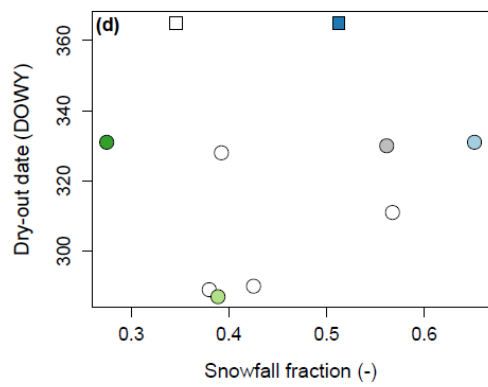
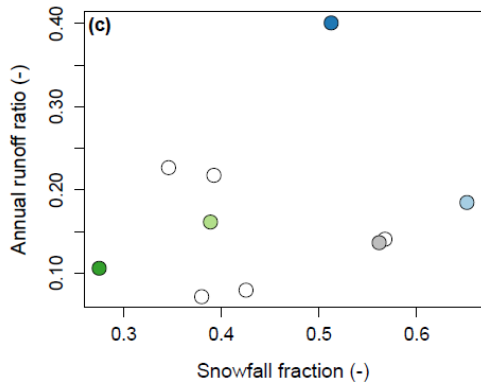
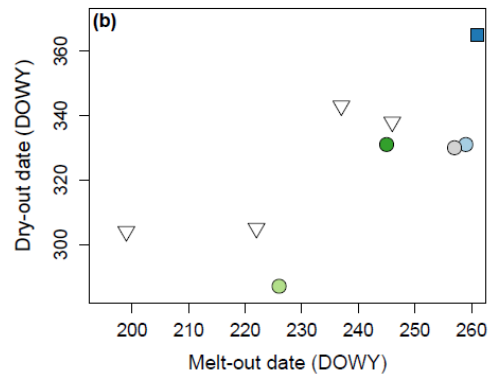
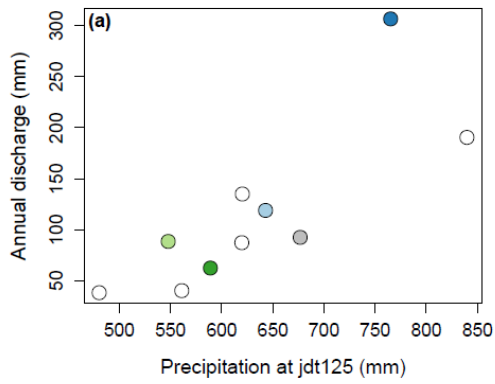
898

899

900

901

Fig. 5 Cumulative surface water inputs (SWI, dashed lines, mm) and discharge (coloured polygons, mm) for each of the water years (dark green = rainy 2005, light blue = snowy 2010, dark blue = wet 2011, light green = dry 2014). Circles indicate the day at which the stream ceased to flow at the catchment outlet (dry-out date, please note that the stream did not cease to flow in 2011) and diamonds indicate the day at which all snow had melted from the catchment (melt-out date).



- Rainy 2005
- Snowy 2010
- Wet 2011
- Dry 2014
- 2009
- other years (2004-2014, Godsey et al., 2018)
- ◇ other years (2016-2019, see section 3.2)
- stream did not fall dry

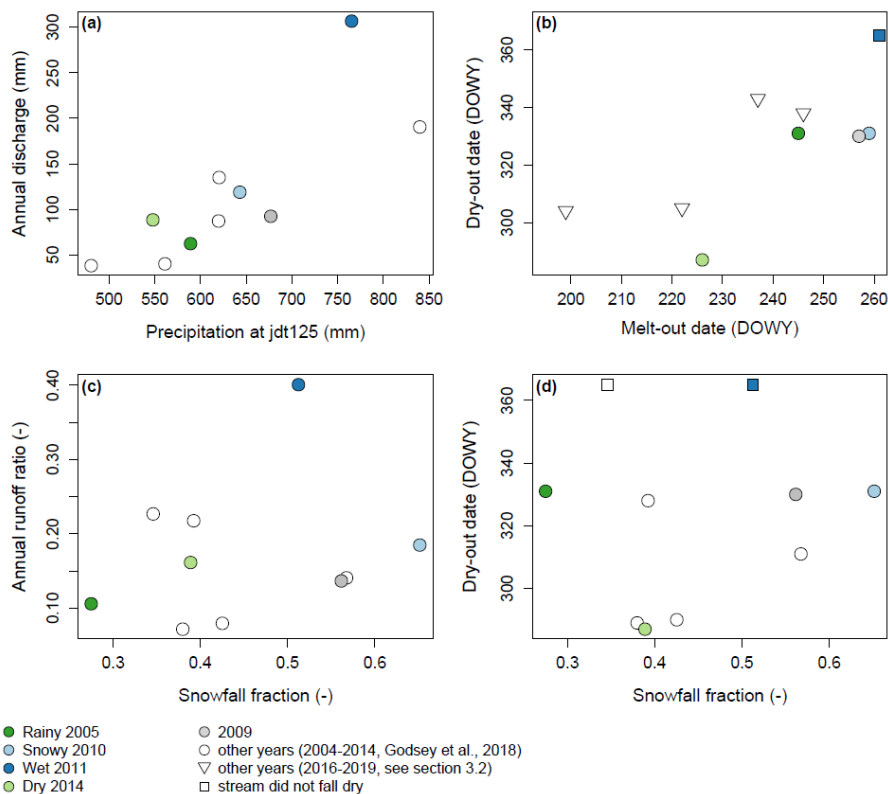
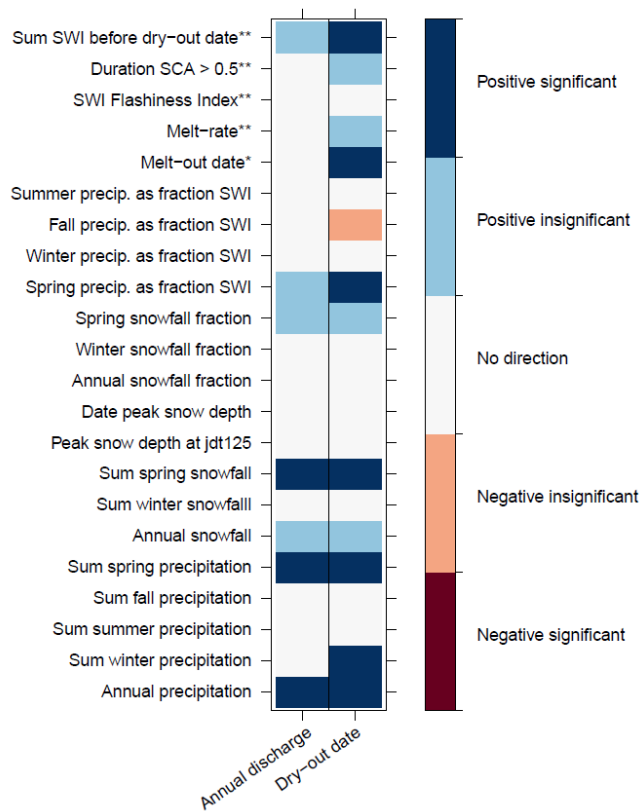


Fig. 6 Scatter plots of (a) annual discharge at the catchment outlet (mm) and annual precipitation at the lowest precipitation gauge (jdt125, mm; see Supplemental Fig. S14 for a comparison with simulated mean catchment precipitation), (b) the day that surface flow in the stream ceased (dry-out date, day of water year (DOWY)) and the day on which all snow had melted (melt-out date, DOWY), (c) annual runoff ratio (annual discharge/annual precipitation at jdt125) and the annual snowfall fraction (-), and (d) the stream dry-out date and the annual snowfall fraction. Years in which the stream did not fall dry out are projected to the last day of the hydrological year. R^2 and p-values for linear regressions between the variables in each panel are: (a) $r^2=0.6083$, $p\text{-value}=0.005001$, (b) $r^2=0.4874$, $p\text{-value}=0.023$, (c) $r^2=-0.0923$, $p\text{-value}=0.607524$, (d) $r^2=-0.1112$, $p\text{-value}=0.790-730$.



913
 914 **Fig. 7: Heatplot showing Pearson correlation coefficients ($\alpha=0.1$) for comparisons between annual discharge, the stream**
 915 **dry-out date and precipitation and snowpack metrics. Significant correlations are marked in dark red (negative) and**
 916 **dark blue (positive), whereas insignificant correlations are marked in light blue (positive) or light red (negative) and**
 917 **correlations without a direction are marked in white ($r < 0.3$). For most metrics, the comparison is based on the**
 918 **2004-2014 data record ($n=11$ years). The comparison with the melt-out date (marked with one asterisk) is based on the**
 919 **simulated years ($n=5$) and the years for which satellite imagery was available (2016-2019, $n=4$; which totals to $n=9$).**
 920 **For the SWI flashiness index, the melt rate, and the number of days when at least half the catchment was snow-covered**
 921 **and the sum of SWI before the dry-out date (marked with two asterisks), we used only the years that were simulated**
 922 **($n=5$). Scatter plots of all significant correlations can be found in Supplemental Fig. S9.**

Formatted: Caption